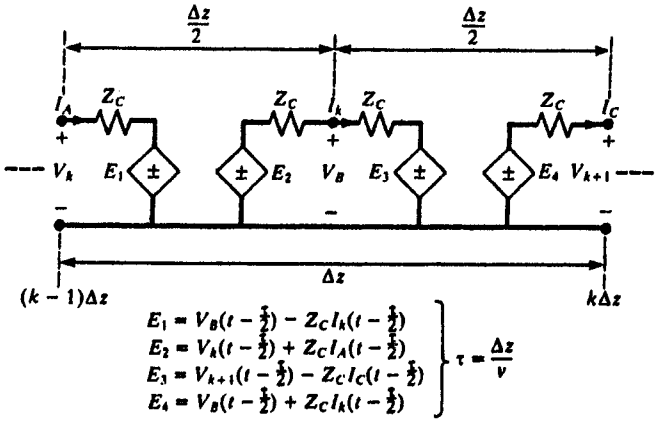


**FIGURE 5.26** Use of Branin's equivalent circuit to prove the exactness of the FDTD current recursion relation at an intermediate point on the line.

$$V_k = -Z_C I_B + D^{-1/2}(V_A + Z_C I_{k-1}) \tag{5.131b}$$

$$V_k = Z_C I_B + D^{-1/2}(V_C - Z_C I_k) \tag{5.131c}$$

$$V_C = -Z_C I_k + D^{-1/2}(V_k + Z_C I_B) \tag{5.131d}$$

Operating on (5.131a) with $D^{1/2}$ and (5.131b) with $D$ and substituting gives

$$DV_k = V_k + 2Z_C D^{1/2} I_{k-1} - Z_C(DI_B + I_B) \tag{5.132}$$

Similarly, operating on (5.131d) with $D^{-1/2}$ and substituting into (5.131c) gives

$$DV_k = V_k - 2Z_C D^{1/2} I_k + Z_C(DI_B + I_B) \tag{5.133}$$

Adding (5.132) and (5.133) gives

$$DV_k = V_k + Z_C D^{1/2}(I_k - I_{k-1}) \tag{5.134}$$

If we substitute the magic time step in (5.122) along with $vc = Z_C^{-1}$ into (5.120b) we obtain (5.134) demonstrating their equivalence. Similarly we can demonstrate the correctness of (5.120d) from the exact circuit model of Fig. 5.26 whose equations are

$$V_k = Z_C I_A + D^{-1/2}(V_B - Z_C I_k) \tag{5.135a}$$

$$V_B = -Z_C I_k + D^{-1/2}(V_k + Z_C I_A) \tag{5.135b}$$

$$V_B = Z_C I_k + D^{-1/2}(V_{k+1} - Z_C I_C) \tag{5.135c}$$

$$V_{k+1} = -Z_C I_C + D^{-1/2}(V_B + Z_C I_k) \tag{5.135d}$$

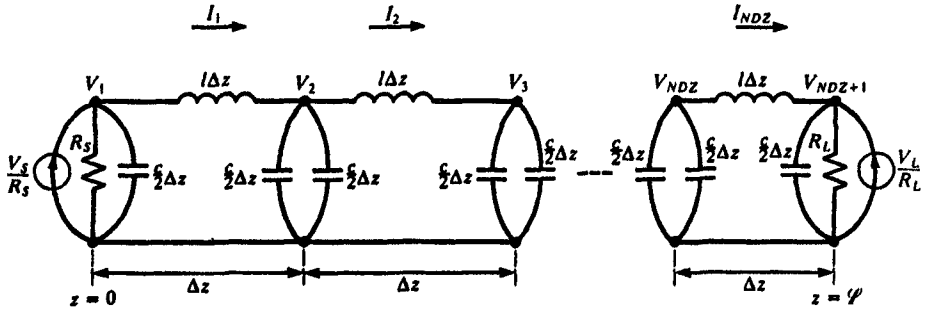


**FIGURE 5.27** Alternative derivation of the FDTD recursion relations using a lumped-pi representation of each section.

The objective is to eliminate $I_A$, $V_B$, $I_C$ from these equations and to show that they are equivalent to (5.120d) for the magic time step of (5.122). Subtracting (5.135a) from (5.135d) and operating on the result with $D$ gives

$$D(V_{k+1} - V_k) = -Z_C D I_C - Z_C D I_A + 2Z_C D^{1/2} I_k \tag{5.136}$$

Operating on (5.135b) and (5.135c) with $D^{3/2}$ and subtracting gives

$$0 = D(V_{k+1} - V_k) - Z_C D I_C - Z_C D I_A + 2Z_C D^{3/2} I_k \tag{5.137}$$

Substituting (5.137) into (5.136) gives

$$D^{3/2} I_k - D^{1/2} I_k = -Z_C^{-1} D(V_{k+1} - V_k) \tag{5.138}$$

Substituting the magic time step of (5.122) along with the fundamental relation $Z_C = vl$ into (5.120d) we obtain (5.138) demonstrating their equivalence.

The above has demonstrated that the finite difference recursion relations given in (5.120) are an exact representation of a two-conductor, lossless line for the magic time step of (5.122). It is possible to provide an alternative, intuitive derivation of those relations in the following manner. A common way of approximating transmission lines, as discussed before, is with the lumped-circuit, iterative approximations. One such representation is the lumped-pi model illustrated in Fig. 4.12(c). Let us use this model and divide the line into $\Delta z$ segments and represent the per-unit-length distributed parameters of inductance and capacitance by lumped elements as shown in Fig. 5.27. The division points are chosen at the above finite difference solution voltages, $V_1$, $V_2, \ldots, V_{NDZ}, V_{NDZ+1}$. Each $\Delta z$ segment is represented by its inductance, $l\Delta z$, and the capacitance is split and placed at the ends of each section as $(c/2)\Delta z$. This illustrates why $(c/2)\Delta z$ is used in the equations for the end segments as pointed out above. The finite difference current solution points, $I_1, I_2, \ldots, I_{NDZ}$,

are through the inductors at the center of the segment. Observing the interlacing of the solution time points according to Fig. 5.22, one can derive equations (5.120) directly from this circuit. This shows that, although (5.120) was derived for resistive terminations, it can be extended to include dynamic terminations so long as the derivatives in those relations are approximated according to Fig. 5.22. Similarly, line losses and incident field effects can be incorporated using Fig. 5.27 and Fig. 5.22 as a guide for their discretization.

As an example, consider the two-conductor lossless line considered earlier and shown in Fig. 5.5. The exact solution for the load voltage, $V(\mathscr{L}, t)$, is sketched by hand in Fig. 5.5(b) and the SPICE results (using a 30 V source voltage with a 0.1 μs rise time) are sketched in Fig. 5.9(a). In the following computed results we will designate

$$\Delta z = \frac{\mathscr{L}}{NDZ}$$

$$\Delta t = \frac{\text{final solution time}}{NDT}$$

The Courant condition given in (5.121) for stability of the FDTD solution given in (5.120) translates to

$$NDT \geq NDZ \frac{v \times \text{final solution time}}{\mathscr{L}}$$

The magic time step in (5.122) occurs for an equality in this expression. Figure 5.28(a) shows the FDTD predictions for zero risetime and $NDZ = 200$ or $\Delta z = 2$ m and the magic time step of $\Delta t = \Delta z/v = 10$ ns. For a final solution time of 20 μs, this gives 2000 time steps or $NDT = 2000$. The results are *exactly* those for the hand calculations. If we reduce the time step below that of the magic time step using 4000 time steps or $\Delta t = 5$ ns we observe considerable "ringing" on the leading edge of each transition. The FDTD solution for $NDZ = 1$ (dividing the line into only one section) and the "magic time step" of $NDT = 10$ or $\Delta t = 2$ μs is denoted as X and gives the *exact solution* even for this course gridding of the line! Figure 5.28(b) shows the FDTD predictions for a 0.1 μs risetime and $NDZ = 200$ or $\Delta z = 2$ m and the magic time step of $\Delta t = \Delta z/v = 10$ ns. Again, the results are *exactly* those for the SPICE or hand calculations. If we reduce the time step below that of the magic time step using 4000 time steps or $\Delta t = 5$ ns we observe less "ringing" on the leading edge of each transition than for the zero-risetime solution. The spectrum of this 0.1 μs risetime pulse rolls off at $-40$ dB/decade above $1/\pi\tau_r = 3.18$ MHz [A.3]. So the section length, $\Delta z$, should be electrically short above this, requiring $\Delta z < 6.29$ m. Thus, if we do not wish to use the magic time step, we must further reduce $\Delta z$ to eliminate this ringing.

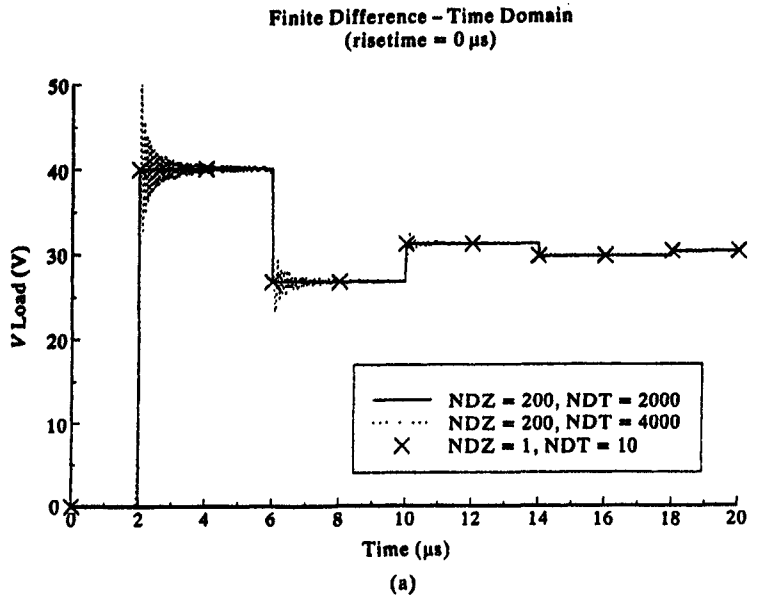


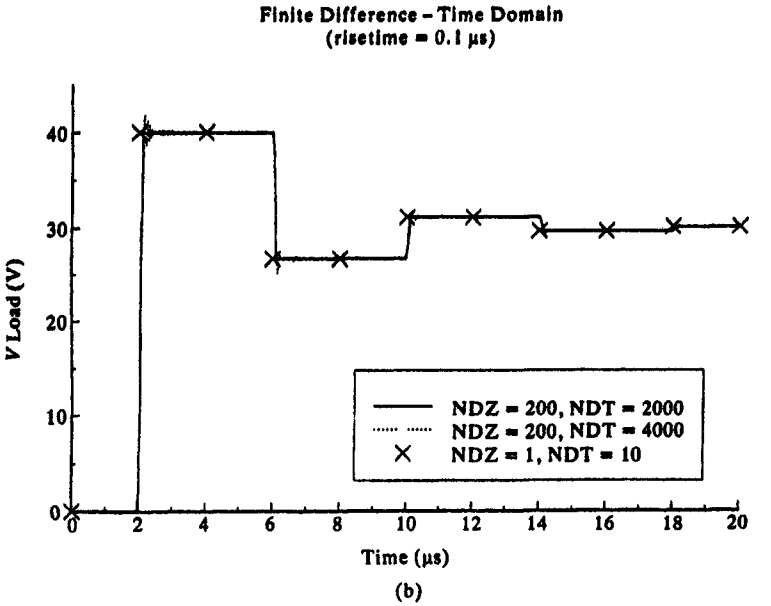


**FIGURE 5.28** Illustration of the computation of the load voltage of Fig. 5.5 using the FDTD method and comparison of the convergence to the choice of spatial and temporal discretization: (a) step response, (b) risetime of 0.1 μs.

Therefore we have demonstrated that the finite difference–time domain recursion relations of (5.120) provide the *exact* solution of the transmission-line equations for lossless, two-conductor lines with lumped loads for the magic time step of $\Delta t = \Delta z/v$! It is a simple matter to extend these results to multiconductor lines using matrix notation. Assume that the multiconductor line has lumped terminal source and load, represented as generalized Thévenin equivalents:

$$\mathbf{V}(0, t) = \mathbf{V}_S(t) - \mathbf{R}_S\mathbf{I}(0, t) \tag{5.139a}$$

$$\mathbf{V}(\mathscr{L}, t) = \mathbf{V}_L(t) + \mathbf{R}_L\mathbf{I}(\mathscr{L}, t) \tag{5.139b}$$

The voltages and currents are again interlaced in position and time as in Figs 5.21 and 5.22. The resulting FDTD recursion relations are

$$\mathbf{V}_1^{n+1} = \left(\frac{\Delta z}{\Delta t}\mathbf{R}_S\mathbf{C} + \mathbf{1}\right)^{-1} \times \left[\left(\frac{\Delta z}{\Delta t}\mathbf{R}_S\mathbf{C} - \mathbf{1}\right)\mathbf{V}_1^n - 2\mathbf{R}_S\mathbf{I}_1^{n+1/2} + (\mathbf{V}_S^{n+1} + \mathbf{V}_S^n)\right] \tag{5.140a}$$

$$\mathbf{V}_k^{n+1} = \mathbf{V}_k^n - \frac{\Delta t}{\Delta z}\mathbf{C}^{-1}(\mathbf{I}_k^{n+1/2} - \mathbf{I}_{k-1}^{n+1/2}) \quad k = 2, \ldots, NDZ \tag{5.140b}$$

$$\mathbf{V}_{NDZ+1}^{n+1} = \left(\frac{\Delta z}{\Delta t}\mathbf{R}_L\mathbf{C} + \mathbf{1}\right)^{-1} \times \left[\left(\frac{\Delta z}{\Delta t}\mathbf{R}_L\mathbf{C} - \mathbf{1}\right)\mathbf{V}_{NDZ+1}^n + 2\mathbf{R}_L\mathbf{I}_{NDZ}^{n+1/2} + (\mathbf{V}_L^{n+1} + \mathbf{V}_L^n)\right] \tag{5.140c}$$

$$\mathbf{I}_k^{n+3/2} = \mathbf{I}_k^{n+1/2} - \frac{\Delta t}{\Delta z}\mathbf{L}^{-1}(\mathbf{V}_{k+1}^{n+1} - \mathbf{V}_k^{n+1}) \qquad k = 1, \ldots, NDZ \tag{5.140d}$$

These equations are implemented in the FORTRAN program **FINDIF.FOR** described in Appendix A.

### 5.2.6 Computed Results

In this section we will give some predicted and experimentally obtained results for the ribbon cable and printed circuit board configurations investigated earlier. The terminal configurations for both structures are shown in Fig. 5.29(a). A 50 Ω time-domain source produces an open-circuit voltage, $V_S(t)$, shown in Fig. 5.29(b) consisting of a trapezoidal periodic pulse train with a 50% duty cycle and equal rise and fall times, $\tau_r = \tau_f$, with various values. We will show results for rise/fall times that are of the order of the one-way time delay, $T = \mathscr{L}/v$, and greater. The level of the pulse will be $V_S = 1$ V in all cases.

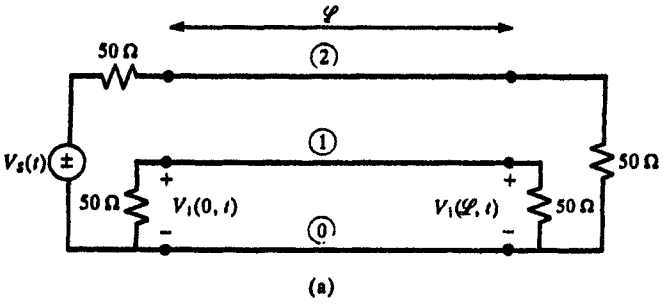


(a)

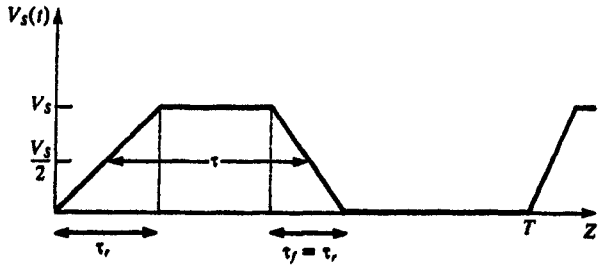


(b)

**FIGURE 5.29** A three-conductor line for illustrating the predictions of various models: (a) terminal representations and (b) representation of the open-circuit voltage waveform of the source.

These are characterized as generalized Thévenin equivalents:

$$\mathbf{V}(0, t) = \mathbf{V}_S(t) - \mathbf{R}_S\mathbf{I}(0, t)$$
$$\mathbf{V}(\mathscr{L}, t) = \mathbf{V}_L(t) + \mathbf{R}_L\mathbf{I}(\mathscr{L}, t)$$

where

$$\mathbf{V}_S(t) = \begin{bmatrix} 0 \\ V_S(t) \end{bmatrix}$$
$$\mathbf{R}_S = \begin{bmatrix} 50 & 0 \\ 0 & 50 \end{bmatrix}$$
$$\mathbf{V}_L(t) = \begin{bmatrix} 0 \\ 0 \end{bmatrix}$$
$$\mathbf{R}_L = \begin{bmatrix} 50 & 0 \\ 0 & 50 \end{bmatrix}$$

Two configurations of a three-conductor line ($n = 2$) are considered: a three-wire ribbon cable and a three-conductor printed circuit board. Experimentally

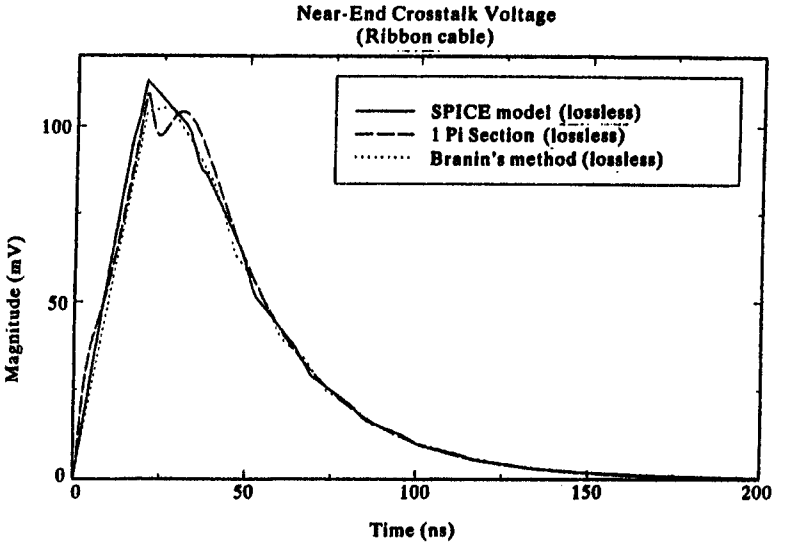


FIGURE 5.30 Comparison of the time-domain response of the near-end crosstalk voltage of the ribbon cable of Fig. 4.14 determined via the SPICE model, the lumped-pi model, and Branin's method implemented directly for a pusle risetime of 20 ns.

determined responses for the *near-end voltage* of line #1, $V_1(0, t)$, will be compared to the predictions of the SPICE model (**SPICEMTL.FOR**), one lumped-pi section (**SPICELPI.FOR**), Branin's method (**BRANIN.FOR**), the time-domain to frequency-domain method (**TIMEFREQ.FOR**), and the finite difference–time domain method (**FINDIF.FOR**). The names in parentheses denote the appropriate FORTRAN program described in Appendix A which implements that method.

*5.2.6.1 Ribbon Cable* The cross section of the three-wire ribbon cable is shown in Fig. 4.14. The pulse risetime will be $\tau_r = 20$ ns. The line length is $\mathscr{L} = 2$ m so that the one-way delay (ignoring the dielectric insulations) is $T = 6.67$ ns. The per-unit-length parameters for this configuration were computed using the computer program **RIBBON.FOR** described in Appendix A and are given in Chapter 3:

$$\mathbf{L} = \begin{bmatrix} 0.748\,50 & 0.507\,7 \\ 0.507\,7 & 1.015\,4 \end{bmatrix} \mu\text{H/m}$$

$$\mathbf{C} = \begin{bmatrix} 34.432 & -18.716 \\ -18.716 & 24.982 \end{bmatrix} \text{pF/m}$$

Figure 5.30 shows a comparison of the predictions of the SPICE model, one lumped-pi section, and Branin's method for a risetime of $\tau_r = 20$ ns. The

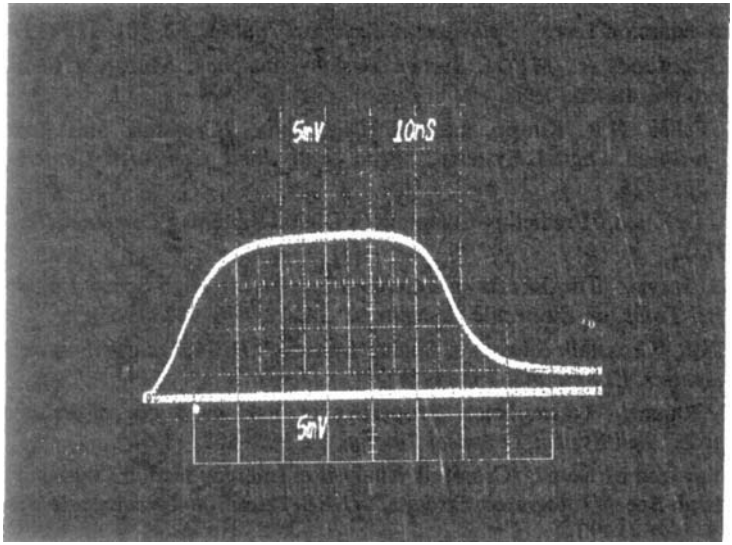


**FIGURE 5.31** Experimentally determined crosstalk for the ribbon cable and a pulse risetime of 20 ns.

experimentally determined response is shown in Fig. 5.31. The experimental results give a peak voltage at 20 ns of some 110 mV. The SPICE model predicts 113 mV and the lumped-pi model predicts 109.1 mV. Branin's method predicts a value of 104 mV. Both the SPICE model and Branin's method are exact (for a lossless line as assumed here) and should show the same values. The fact that they do not is due to the fact that the per-unit-length parameters of the SPICE model include the dielectric inhomogeneity whereas Branin's method can only be used for a homogeneous medium. The inductance matrices for both cases are, of course, identical since the dielectric does not affect this parameter. Using the capacitance matrix with the dielectric removed, $\mathbf{C}_o$, computed in Chapter 3:

$$\mathbf{C}_o = \begin{bmatrix} 22.494 & -11.247 \\ -11.247 & 16.581 \end{bmatrix} \text{pF/m}$$

along with **L** in the SPICE model gives the identical comparison shown in Fig. 5.32 which confirms this hypothesis. Figure 5.33 shows the predictions of the time-domain to frequency-domain method using **TIMEFREQ.FOR** and a frequency-domain transfer function (computed using the FORTRAN program **MTL.FOR** without considering losses) computed for 100, 50, 20, and 10 harmonics of the fundamental frequency, $f_o = 1$ MHz. (Actually it doesn't matter what repetition frequency or duty cycle or fall time is used so long as the response to the rising edge, which is shown in the figure, has died out

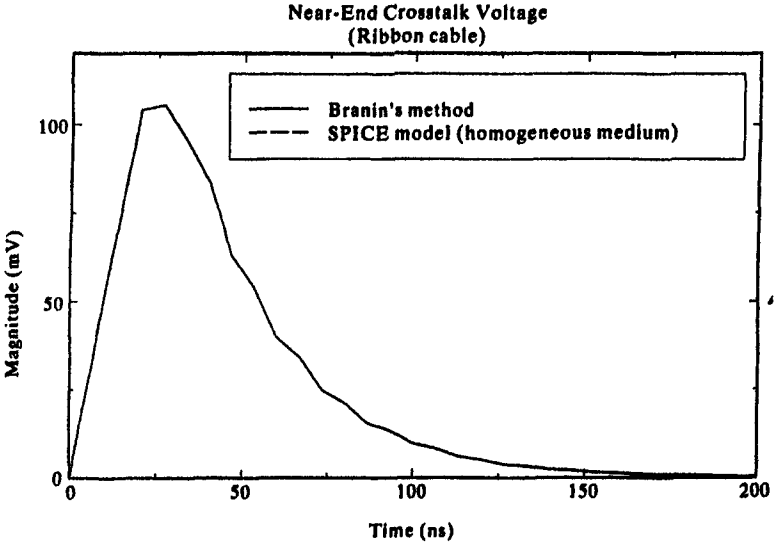


FIGURE 5.32 Comparison of the predictions of the SPICE model (for a homogeneous medium) and Branin's method implemented directly for the ribbon cable showing the effect of the wire insulation dielectric. Pulse risetime = 20 ns.

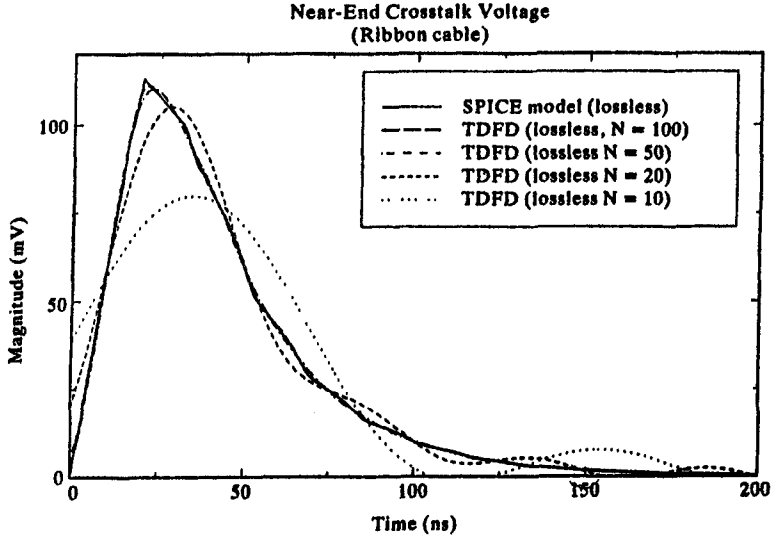


FIGURE 5.33 Comparison of the predictions of the SPICE model and the time-domain to frequency-domain transformation method for the ribbon cable. Pulse risetime = 20 ns.

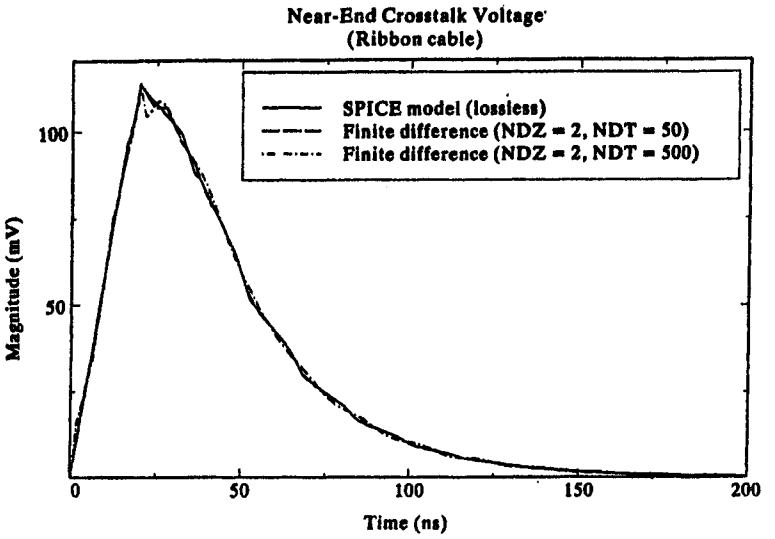


**FIGURE 5.34** Comparison of the predictions of the SPICE model and the FDTD method for the ribbon cable.

sufficiently.) The predictions using 100 and 50 harmonics are virtually identical to the exact SPICE results. The predictions using 20 and 10 harmonics are not so good. This is because the spectrum of the pulse begins to roll off at a rate of $-40$ dB/decade above a frequency of $f = 1/\pi\tau_r = 15.9$ MHz [A.3]. Thus for a fundamental frequency of 1 MHz, the twentieth harmonic is at 20 MHz and the frequency response at the frequencies above this apparently contribute significantly to the response.

Figure 5.34 shows the predictions of the finite difference–time domain model using **FINDIF.FOR** versus the exact SPICE results. Two discretizations are shown. The mode velocities computed with **SPICEMTL.FOR** are $v_1 = 2.323\,97 \times 10^8$ m/s and $v_2 = 2.510\,64 \times 10^8$ m/s. Since the spectrum of the pulse rolls off at $-40$ dB/decade above $f = 1/\pi\tau_r = 15.9$ MHz we choose $\Delta z = 1$ m from the smaller mode velocity giving $NDZ = 2$ so that each section is electrically short above around 25 MHz. To use the magic time step, we choose, for a final solution time of 200 ns, 50 time steps corresponding to the largest mode velocity, $v_2$. This will insure that we are in the stable range of the Courant condition for the smaller mode velocity, $v_1$. The comparison with the SPICE results (which are exact) is excellent. Even though we reduce the time step below the magic time step the predictions are still quite good.

In Chapter 4 it was pointed out that in order to match a MTL consisting of more than two conductors ($n > 1$), it is not sufficient to terminate each line to the reference conductor with a *single resistance*. In order to match the line, the termination impedance matrix in the generalized Thévenin characterization

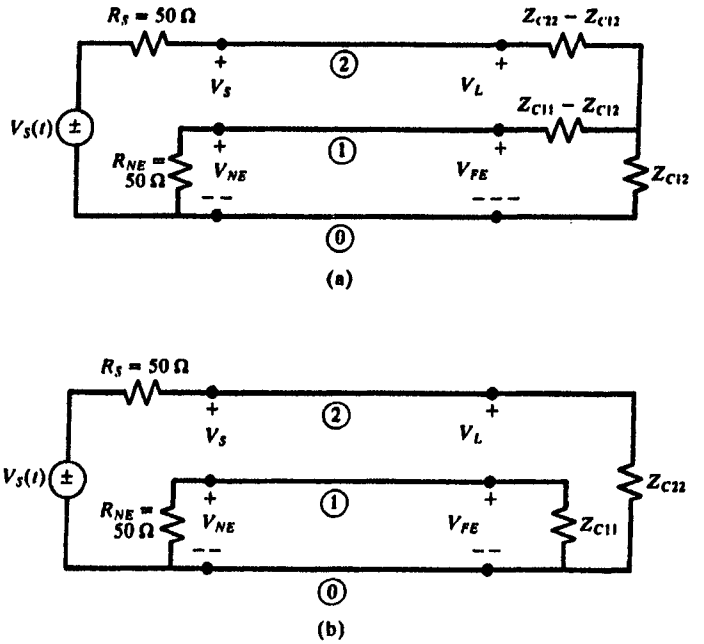


**FIGURE 5.35** Illustration of matching of a MTL for (a) completely matched lines and (b) partially matched lines.

of the termination must equal the characteristic impedance matrix, i.e., $\mathbf{R}_S = \mathbf{Z}_C$ and/or $\mathbf{R}_L = \mathbf{Z}_C$. In order to demonstrate this let us terminate this ribbon cable with a matched termination, i.e., $\mathbf{R}_L = \mathbf{Z}_C$, as shown in Fig. 5.35(a). The characteristic impedance matrix is

$$\begin{aligned}\mathbf{Z}_C &= v_o\mathbf{L} \\ &= \begin{bmatrix} Z_{C11} & Z_{C12} \\ Z_{C12} & Z_{C22} \end{bmatrix} \\ &= \begin{bmatrix} 224.395 & 152.205 \\ 152.205 & 304.409 \end{bmatrix} \Omega\end{aligned}$$

where we will ignore the dielectric insulations and assume a homogeneous medium (free space) with $v_o = 2.997\,925 \times 10^8$ m/s. In order to simulate this termination we insert the resistors as shown in Fig. 5.35(a). (See Problem 4.19.) We will use the SPICE model with $\mathbf{L}$ and $\mathbf{C}_o$ given above. Figure 5.36(a) shows the results of the simulation for the above 1 MHz trapezoidal pulse train with $\tau_r = 20$ ns. Observe that the line is evidently matched with this termination. The question of whether one can *partially match* the line by placing termination

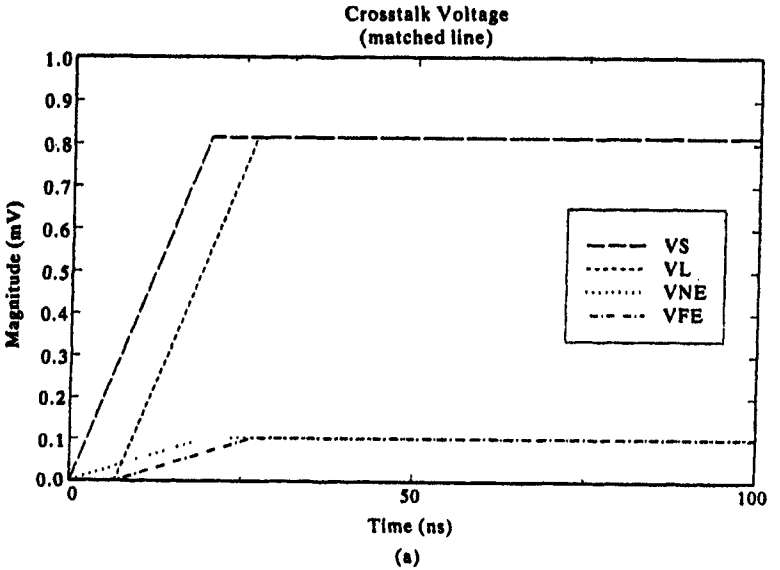


(a)

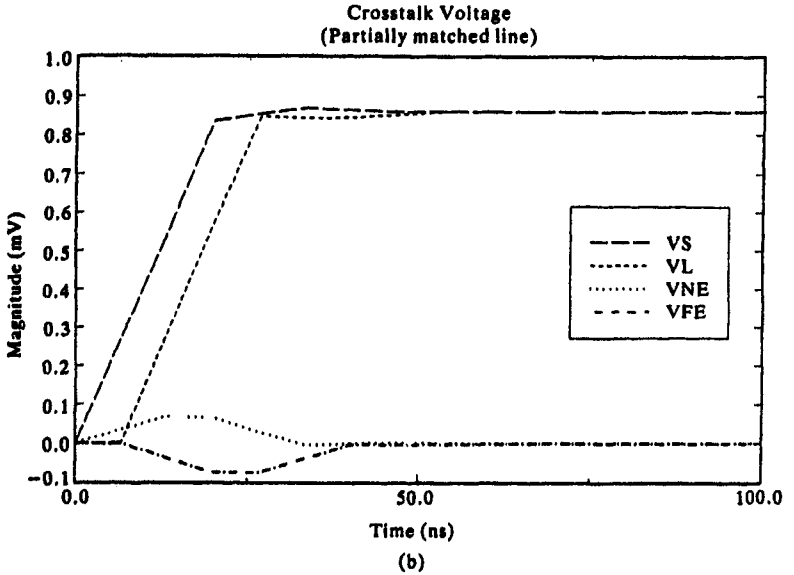


(b)

**FIGURE 5.36** Time-domain voltages for (a) the completely matched line showing no reflections and (b) the partially matched line showing reflections.

resistors $Z_{C11}$ and $Z_{C22}$ *only* between each line and the reference conductor as in Fig. 5.35(b) is investigated next. The results of the simulation of Fig. 5.35(b) are shown in Fig. 5.36(b). Observe that this line is clearly not matched but the results do converge to a steady state quite rapidly. So, ideally, to eliminate all reflections on a MTL it must be terminated in its characteristic impedance matrix, $\mathbf{Z}_C$. However, because there is cross coupling in $\mathbf{Z}_C$ due to $Z_{C12} \neq 0$, this gives a nonzero crosstalk level of about 100 mV, as shown in Fig. 5.36(a), that is not present in results for the partially matched line shown in Fig. 5.36(b). This cross coupling essentially acts like common-impedance coupling through the nonzero $Z_{C12}$ resistance in Fig. 5.35(a). However, this is the price we pay for completely matching the line.

*5.2.6.2 Printed Circuit Board* The remaining structure to be examined is the three-conductor printed circuit board considered previously and shown in cross section in Fig. 4.17. The above methods will be used to predict the response for a 1 MHz trapezoidal pulse train shown in Fig. 5.29 having a rise/fall time of $\tau_r = 6.25$ ns. The line length is $\mathscr{L} = 0.254$ m = 10 inches so that the one-way delay (ignoring the board) is $T = 0.847$ ns. The per-unit-length parameters for this configuration were computed using the computer program **PCBGAL.FOR** described in Appendix A and are given in Chapter 3:

$$\mathbf{L} = \begin{bmatrix} 1.104\,18 & 0.690\,094 \\ 0.690\,094 & 1.380\,19 \end{bmatrix} \mu\text{H/m}$$

$$\mathbf{C} = \begin{bmatrix} 40.628\,0 & -20.314\,0 \\ -20.314\,0 & 29.763\,2 \end{bmatrix} \text{pF/m}$$

A comparison of the predictions of Branin's method, the SPICE model, and one pi section are shown in Fig. 5.37. The predictions of the exact SPICE model and one lumped-pi section are again quite close. Once again, Branin's method shows some error since it effectively ignores the board dielectric and assumes a homogeneous medium (in this case free space). The experimental results are shown in Fig. 5.38. The peak measured voltage is 94 mV compared with a prediction of the SPICE model of 95 mV. Figure 5.39 compares the predictions of the SPICE model and the time-domain to frequency-domain method computed using the code **TIMEFREQ.FOR**. For the risetime of 6.26 ns the spectrum of the pulse begins to roll off at a rate of $-40$ dB/decade above a frequency of $f = 1/\pi\tau_r = 51$ MHz so we should expect to require more than 50 harmonics to achieve convergence as is evident in the plot. Figure 5.40 compares the SPICE predictions to those of the finite difference–time domain model computed using the code **FINDIF.FOR**. The mode velocities are $v_1 = 1.800\,65 \times 10^8$ m/s and $v_2 = 1.922\,36 \times 10^8$ m/s. The $\Delta z$ discretization is again chosen to make each section electrically short at $1/\pi\tau_r = 51$ MHz giving, using the smaller velocity $v_1$, $\Delta z < 0.353$ m. So we choose $NDZ = 2$. Using the larger mode velocity, $v_2$, gives the magic time step of $NDT = 60$. The comparison

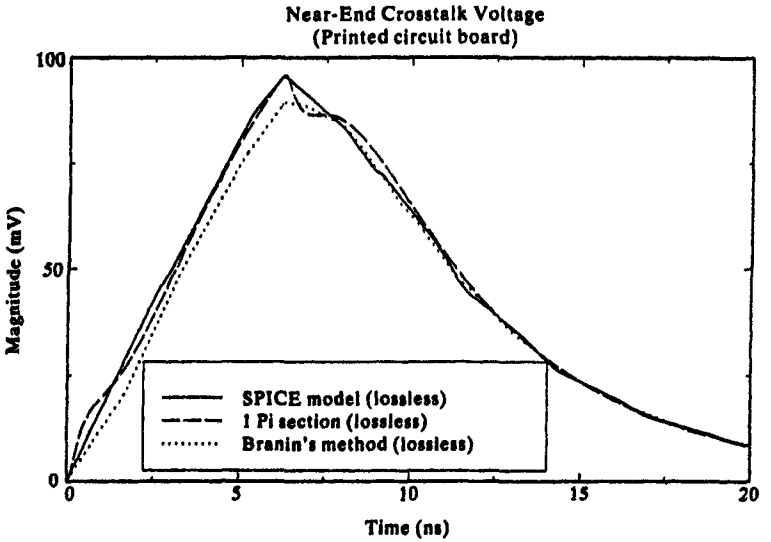


**FIGURE 5.37** Comparison of the time-domain response of the near-end crosstalk of the printed circuit board of Fig. 4.17 determined via the SPICE model, the lumped-pi model, and Branin's method implemented directly for a pulse risetime of 6.25 ns.

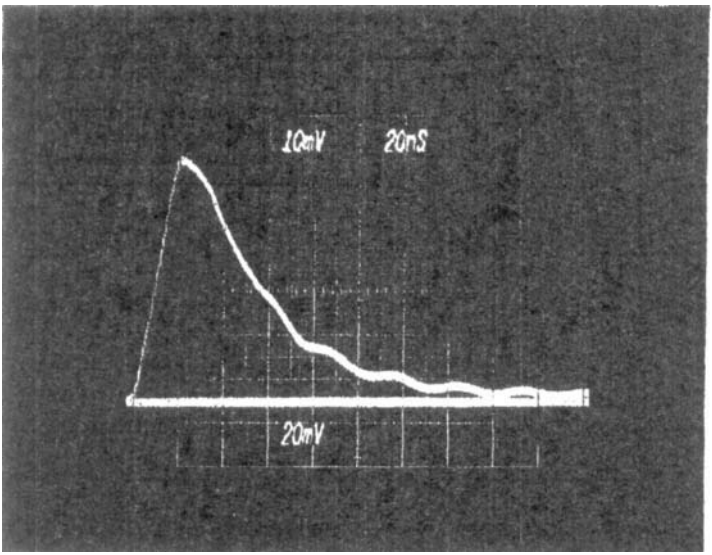


**FIGURE 5.38** Experimentally determined crosstalk for the printed circuit board and a pulse risetime of 6.25 ns.

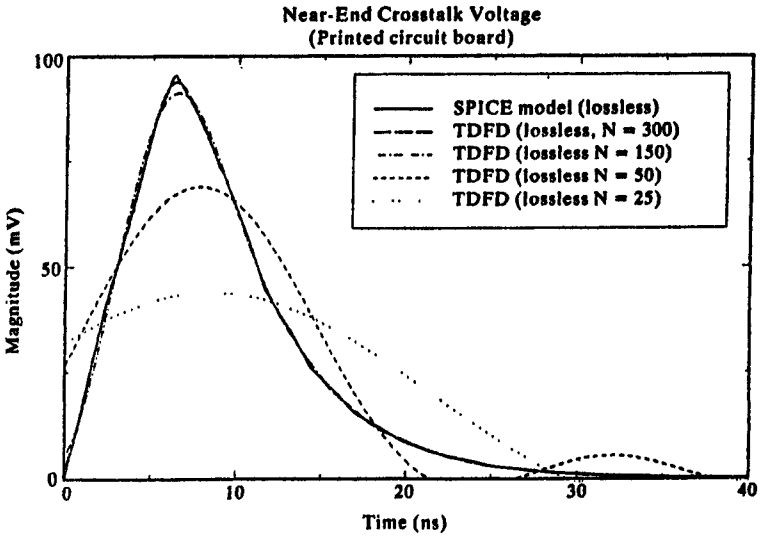


FIGURE 5.39 Comparison of the predictions of the SPICE model and the time-domain to frequency-domain transformation method for the printed circuit board. Pulse risetime = 6.25 ns.

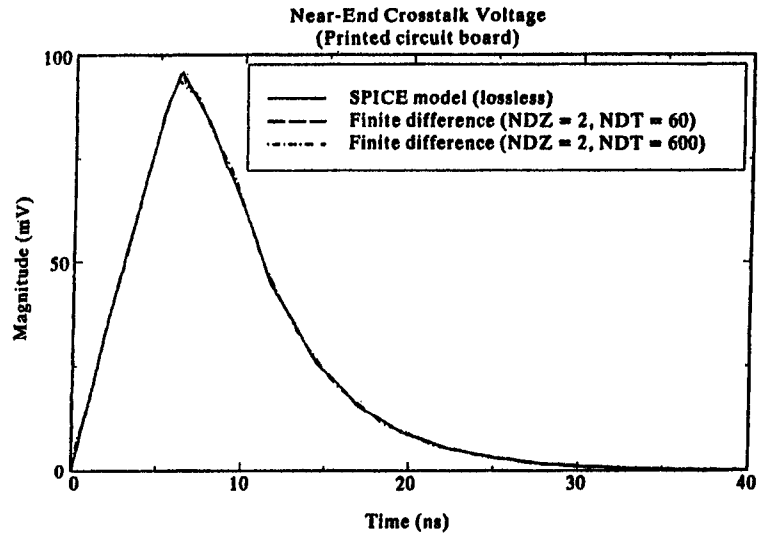


FIGURE 5.40 Comparison of the predictions of the SPICE model and the FDTD method for the printed circuit board. Pulse risetime = 6.25 ns.

between the exact solution and the FDTD solution for the magic time step is excellent. Observe that even when the time discretization is reduced from that of the magic time step, $NDZ = 2$, $NDT = 600$, the correlation remains excellent. This again demonstrates that even in the case of MTL's in inhomogeneous media where the mode velocities are different, and the discretization can be chosen equal to the magic time step for only one of those velocities, the FDTD method can still give adequate results even though the other mode velocities do not satisfy the magic time step condition.

## 5.3 INCORPORATION OF LOSSES

Losses arise from either the nonzero conductivity and polarization loss of the surrounding medium or from imperfect conductors. Of the two mechanisms, the loss introduced by imperfect conductors is usually more significant than the loss due to the medium for typical transmission-line structures. It is for this reason that the surrounding medium is often assumed to be lossless, i.e., set $\mathbf{G} = \mathbf{0}$ in the MTL equations. The resistance due to imperfect conductors is represented in the per-unit-length resistance matrix, **R**. The per-unit-length inductance matrix, **L**, can be separated into a portion, $\mathbf{L}_i$, due to magnetic flux internal to the conductors and a portion, $\mathbf{L}_e$, due to magnetic flux external to the conductors as $\mathbf{L} = \mathbf{L}_i + \mathbf{L}_e$. In the case of perfect conductors, the current flows on the conductor surfaces and the internal inductance is zero: $\mathbf{L} = \mathbf{L}_e$.

In Chapter 3 we discussed the per-unit-length resistance and internal inductance for conductors. At the lower frequencies where the skin depth, $\delta = 1/\sqrt{\pi f \mu \sigma}$, is much larger than the conductor cross-sectional dimensions, the resistance and internal inductance are constant and equal the dc values because the current may be assumed to be uniformly distributed over the cross section. At the higher frequencies where the skin depth is much smaller than the conductor cross section the resistance increases as $\sqrt{f}$ and the internal inductance decreases as $\sqrt{f}$ because the current crowds to the outer edges of the conductor cross section and can be represented, as an approximation, to be uniformly distributed over a strip at the surface of thickness equal to one skin depth and zero elsewhere. This is exact for a conductor of circular cross section (a wire) in the absence of neighboring conductors, but for a conductor of rectangular cross section, such as a PCB land, the current crowds to the corners so that this underestimates the resistance as we saw in Chapter 3. Thus the entries in **R** are constant at lower frequencies and increase as $\sqrt{f}$ at the higher frequencies. The entries in the per-unit-length inductive reactance matrix, $\omega\mathbf{L}$, are the sum of the internal inductive reactance matrix, $\omega\mathbf{L}_i$, and the external inductive reactance matrix, $\omega\mathbf{L}_e$. At the lower frequencies, the internal inductance is constant, and at the higher frequencies it decreases as $\sqrt{f}$ so that the entries in the internal inductive reactance, $\omega\mathbf{L}_i$, increase as $\sqrt{f}$ at the higher frequencies.

In the frequency domain, the MTL equations can be written as

$$\frac{d}{dz}\hat{\mathbf{V}}(z) = -[\hat{\mathbf{Z}}_i(\omega) + j\omega\mathbf{L}]\hat{\mathbf{I}}(z) \tag{5.141a}$$

$$\frac{d}{dz}\hat{\mathbf{I}}(z) = -[\mathbf{G} + j\omega\mathbf{C}]\hat{\mathbf{V}}(z) \tag{5.141b}$$

where $\mathbf{L}$ represents the external inductance, and the internal inductance is included in $\hat{\mathbf{Z}}_i(\omega) = \mathbf{R} + j\omega\mathbf{L}_i$. To obtain the time-domain results we represent the MTL equations with the Laplace transform as

$$\frac{d}{dz}\mathbf{V}(z, s) = -[\mathbf{Z}_i(s) + s\mathbf{L}]\mathbf{I}(z, s) \tag{5.142a}$$

$$\frac{d}{dz}\mathbf{I}(z, s) = -[\mathbf{G} + s\mathbf{C}]\mathbf{V}(z, s) \tag{5.142b}$$

A common way of approximating the internal impedance term with the Laplace transform variable is as [14, 15]

$$\mathbf{Z}_i(s) = \mathbf{A} + \mathbf{B}\sqrt{s} \tag{5.143}$$

That this represents a reasonable approximation to the skin effect behavior can be seen if we substitute $s = j\omega$ to yield

$$\begin{aligned}\hat{\mathbf{Z}}_i(\omega) &= \mathbf{A} + \mathbf{B}\sqrt{j\omega} \\ &= \mathbf{A} + \mathbf{B}\sqrt{\pi}\sqrt{f}(1 + j)\end{aligned} \tag{5.144}$$

Thus $\mathbf{A}$ represents the dc per-unit-length resistance matrix. The component $\mathbf{B}\sqrt{\pi}\sqrt{f}(1 + j)$ represents the high-frequency per-unit-length resistance matrix as well as the high-frequency per-unit-length internal inductive reactance matrix. This assumes that the high-frequency resistance and internal inductive reactance are equal, which can be shown to be true for all conductor cross sections using Wheeler's "incremental inductance rule" (see reference [28] in Chapter 3). Although it may appear that we may include the dc internal inductance in the inductance matrix, $\mathbf{L}$, this is not possible for the following reason. Above a frequency $f_o$ the internal inductance *decreases* as $\sqrt{f}$. If we simply added the dc internal inductance to $\mathbf{L}$, this would dominate the high-frequency internal inductance (which decreases as $\sqrt{f}$) and we would effectively be ignoring this behavior at the high frequencies, which would affect the early-time response and artificially change the time delay of the line. The approximation in (5.143) stems from the observation that for low frequencies,

where the skin effect is not well developed, the dc values dominate the high-frequency values, where the skin effect is well developed, and vice-versa. This is shown for wires in Figs 3.52 and 3.53, and for conductors of rectangular cross section in Fig. 3.58. Consequently the per-unit-length impedance of the conductor is modeled as

$$\begin{aligned} \hat{z}_l(\omega) &= A + B\sqrt{j\omega} \\ &= r_{dc} + r_{hf} + j\omega l_{l,hf} \\ &= r_{dc} + r_{dc}\sqrt{\frac{f}{f_o}}\,(1+j). \end{aligned}$$

The inaccuracy in this approximation occurs where the impedance transitions from the low-frequency value to the high-frequency value at $f_o$. In order to obtain the quantities A and B for typical conductors, consider a wire or radius $r_w$. From (3.202) we observe that

$$A = r_{dc} = \frac{1}{\sigma \pi r_w^2}$$

$$B = \frac{1}{2\pi r_w}\sqrt{\frac{\mu}{\sigma}}$$

The resistance of the reference conductor would be similarly added to all entries of A. Similarly, for a conductor of rectangular cross section having width $w$ and thickness $t$, the approximations given in (3.220) and (3.221) yield

$$A = r_{dc} = \frac{1}{\sigma w t}$$

$$B = \frac{1}{2(t+w)}\sqrt{\frac{\mu}{\sigma}}$$

There is one final observation apparent in (5.142). The product of two Laplace-transformed variables translates in the time domain to the convolution of their time-domain representations [A.2]:

$$X(s)Y(s) \Leftrightarrow x(t) * y(y) = \int_{-\infty}^{\infty} x(t-\tau)y(\tau)\,d\tau \tag{5.145}$$

Therefore, (5.142) translates in the time domain to

$$\frac{\partial}{\partial z}\mathbf{V}(z,t) = -\mathbf{Z}_l(t) * \mathbf{I}(z,t) - \mathbf{L}\frac{\partial}{\partial t}\mathbf{I}(z,t) \tag{5.146a}$$

$$\frac{\partial}{\partial z}\mathbf{I}(z,t) = -\mathbf{G}\mathbf{V}(z,t) - \mathbf{C}\frac{\partial}{\partial t}\mathbf{V}(z,t) \tag{5.146b}$$

This shows that the high-frequency skin-effect resistance and internal inductance that vary as $\sqrt{f}$ require a convolution of the time-domain representation, $\mathbf{Z}_i(t)$, and the line currents as was pointed out in [16]. The explicit representation of (5.146a) can be obtained in the following way. Expanding (5.142a) using the approximation given in (5.143) yields

$$\frac{d}{dz}\mathbf{V}(z,s) = -[\mathbf{A} + \mathbf{B}\sqrt{s}]\mathbf{I}(z,s) - s\mathbf{L}\mathbf{I}(z,s) \tag{5.147}$$

$$= -\mathbf{A}\mathbf{I}(z,s) - \mathbf{B}\left[\frac{1}{\sqrt{s}}\right]s\mathbf{I}(z,s) - s\mathbf{L}\mathbf{I}(z,s)$$

The skin-effect term is placed in the form of $\sqrt{s} = s/\sqrt{s}$ to simplify the result since the inverse transform of $1/\sqrt{s}$ is [16, 17]

$$\frac{1}{\sqrt{s}} \Leftrightarrow \frac{1}{\sqrt{\pi}}\frac{1}{\sqrt{t}} \tag{5.148}$$

Therefore the result simplifies to

$$\frac{\partial}{\partial z}\mathbf{V}(z,t) = -\mathbf{Z}_i(t) * \mathbf{I}(z,t) - \mathbf{L}\frac{\partial}{\partial t}\mathbf{I}(z,t) \tag{5.149}$$

$$= -\mathbf{A}\mathbf{I}(z,t) - \frac{1}{\sqrt{\pi}}\mathbf{B}\left[\int_0^t \frac{1}{\sqrt{\tau}}\frac{\partial}{\partial(t-\tau)}\mathbf{I}(z,t-\tau)\,d\tau\right] - \mathbf{L}\frac{\partial}{\partial t}\mathbf{I}(z,t)$$

Observe that this result shows that the convolution integral requires knowledge of the entire past history of (the derivative of) the current. Of course there are various approximate ways of including skin-effect losses that avoid this operation; these we will also investigate.

### 5.3.1 Two-Conductor Lossy Lines

In the case of two-conductor lines the MTL equations and the results in (5.141) to (5.149) reduce to scalars and the transmission-line equations become:

$$\frac{d}{ds}V(z,s) = -[A + B\sqrt{s} + sL]I(z,s) \tag{5.150a}$$

$$\frac{d}{ds}I(z,s) = -[G + sC]V(z,s) \tag{5.150b}$$

Many of the MTL results are extensions of the results obtained for two-conductor lines which we now investigate.

***5.3.1.1 Lumped-Circuit Approximate Characterizations*** Perhaps the simplest way of including losses is via an approximate lumped-circuit model. The obvious structural choices are the lumped-pi or lumped-T structures investigated previously. The advantage of these representations is that simple lumped-circuit analysis programs can be used to solve for the line voltages either in the frequency domain or the time domain. The primary difficulty with these approximations is that they do not correctly process certain of the high-frequency spectral components of the input signal because their validity is based on the assumption that they are electrically short at *all* frequencies of interest. Figure 5.41(a) shows a lumped-pi representation of a section of the line. Typically this type of representation requires a large number of such sections to represent the line for input signals having significant high-frequency spectral content. Implementation of this lumped-circuit approximation is straightforward if we omit consideration of the skin-effect $\sqrt{f}$ behavior of the line resistance (and internal inductance) and only include the dc resistance and internal inductance which can be represented as constant elements.

A recurring problem is how we shall represent the $\sqrt{f}$ skin-effect behavior in the time domain which is required in these lumped-circuit representations. A novel method of doing this is to simulate the physical process that occurs in the development of the skin effect [18]. For a conductor of circular cross section the current resides in annuli and is more strongly concentrated in the outer annuli as frequency is increased. Each of these annuli can be represented by a resistor and an inductor. The circuit representation of this process shown in Fig. 5.41(b) serves to simulate this process. At dc all resistors are in parallel giving the dc resistance. As frequency increases, each branch is successively removed from the circuit generating a $\sqrt{f}$ frequency dependence. Of course, a larger number of branches is required to extend this $\sqrt{f}$ behavior to higher frequencies. Another representation that is particularly useful for conductors of rectangular cross section is to simulate the representation of the conductor as numerous bars in parallel as shown in Fig. 3.56. The current over each subbar is assumed constant but of unknown value and the dc resistances and partial inductances of the individual subbars are used to give the circuit shown in Fig. 5.41(c); this was implemented in [19]. Because of the interaction between the subbars via the mutual partial inductances, the currents in the subbars adjust to simulate the actual skin effect that occurs.

The FORTRAN code **SPICELPI.FOR** described in Appendix A for lossless lines generates a lumped-pi SPICE subcircuit model. This can be then modified to include losses by adding either dc resistances or one of the skin-effect simulations in Fig. 5.41(b) or (c). In this way only the line is modeled and nonlinear loads can be handled in the CAD code in which this model is imbedded. This is a simple approximation but suffers from the lengthy

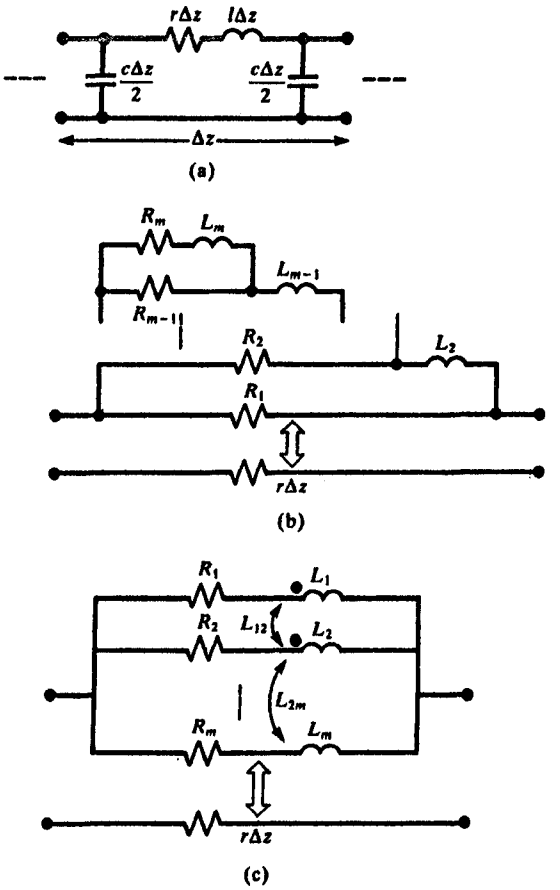


**FIGURE 5.41** Representation of skin-effect $\sqrt{f}$ conductor internal impedance: (a) the lumped-pi model, (b) approximation of the internal impedance as a frequency-selective network, and (c) approximation of the internal impedance via the method of coupled subconductors.

computation time which a sufficiently large circuit model requires to model the very-high-frequency spectral components of the input signal.

*5.3.1.2 Time-Domain to Frequency-Domain Transformations* Once again, a very straightforward way of including losses, particularly $\sqrt{f}$ skin-effect losses, that are difficult to model directly in the time domain, is the time-domain to frequency-domain transformation. The frequency-domain transfer function (magnitude and phase) between the input and the desired output is obtained with the frequency-domain methods of Chapter 4. Observe that all of the line terminations are imbedded in this transfer function. Thus if any of the

terminations are *nonlinear*, the overall system is *nonlinear* and the notion of a frequency-domain transfer function is not useful. Skin-effect $\sqrt{f}$ dependence causes no complications in the frequency-domain computation of the transfer function. The Fourier transform or the Fourier series of the input signal is obtained, and its individual spectral components are passed through the frequency-domain transfer function to yield the spectral components of the output. The time-domain output is the inverse Fourier transform of this spectrum. This straightforward technique is implemented in the FORTRAN code **TIMEFREQ.FOR** described in Appendix A which uses the frequency-domain transfer function computed with **MTL.FOR**. This method requires that the frequency-domain transfer function be computed at a sufficient number of frequencies of the input spectrum. It is a very simple and often-used method of indirectly determining the time-domain response but suffers from the basic restriction that a linear line and terminations are required since superposition was implicitly used.

***5.3.1.3 Finite Difference–Time Domain (FDTD) Methods*** The next rather obvious method is the finite difference–time domain (FDTD) method described earlier for lossless lines. This can be straightforwardly adapted to handle losses including $\sqrt{f}$ skin-effect dependence [20, 21]. The FDTD discretization of the transmission-line equations are given earlier in (5.115). The only change in the discretization of these equations is in the voltage change equation (5.115a) which requires the addition of the discretized convolution term shown in (5.149). The term containing the constant, $A$, representing the conductor dc resistance can be represented in the usual fashion as the average of the currents about the present cellular point as shown in (5.115a). The convolution term can be discretized in the following fashion. Divide the time axis into $\Delta t$ segments. Kunz showed that the discrete convolution can be approximated in the following manner assuming that the function $F(t)$ may be approximated as being constant over the $\Delta t$ segments [21]:

$$\int_0^t \frac{1}{\sqrt{\tau}} F(t-\tau)\, d\tau \cong \int_0^{(n+1)\Delta t} \frac{1}{\sqrt{\tau}} F((n+1)\Delta t - \tau)\, d\tau \tag{5.151a}$$

$$\cong \sum_{m=0}^{n} F^{n+1-m} \int_{m\Delta t}^{(m+1)\Delta t} \frac{1}{\sqrt{\tau}}\, d\tau$$

$$\cong \sqrt{\Delta t} \sum_{m=0}^{n} F^{n+1-m} Z_0(m)$$

where

$$Z_0(m) = \int_m^{(m+1)} \frac{1}{\sqrt{s}}\, ds \tag{5.151b}$$

Adapting this result to the discretization of the transmission-line equation gives,

with reference to Fig. 5.22,

$$\frac{V_{k+1}^{n+1} - V_k^{n+1}}{\Delta z} + l\frac{I_k^{n+3/2} - I_k^{n+1/2}}{\Delta t} + A\frac{I_k^{n+3/2} + I_k^{n+1/2}}{2} + \frac{\sqrt{\Delta t}}{\sqrt{\pi}} B \sum_{m=0}^{n} \left(\frac{I_k^{n+3/2-m} - I_k^{n+1/2-m}}{\Delta t}\right) Z_0(m) = \frac{V_{Fk}^{n+3/2} + V_{Fk}^{n+1/2}}{2} \tag{5.152a}$$

$$\frac{I_k^{n+1/2} - I_{k-1}^{n+1/2}}{\Delta z} + c\frac{V_k^{n+1} - V_k^n}{\Delta t} + g\frac{V_k^{n+1} + V_k^n}{2} = \frac{I_{Fk}^{n+1} + I_{Fk}^n}{2} \tag{5.152b}$$

Only the first equation has changed from the previous discretization. Solving (5.152a) gives the recursion relation for this equation:

$$\left(l\frac{\Delta z}{\Delta t} + A\frac{\Delta z}{2} + B\frac{\Delta z}{\sqrt{\pi \Delta t}} Z_0(0)\right) I_k^{n+3/2} \tag{5.153}$$

$$= \left(l\frac{\Delta z}{\Delta t} - A\frac{\Delta z}{2} + B\frac{\Delta z}{\sqrt{\pi \Delta t}} Z_0(0)\right) I_k^{n+1/2}$$

$$- B\frac{\Delta z}{\sqrt{\pi \Delta t}} \sum_{m=1}^{n} (I_k^{n+3/2-m} - I_k^{n+1/2-m}) Z_0(m)$$

$$- (V_{k+1}^{n+1} - V_k^{n+1}) + \frac{\Delta z}{2}(V_{Fk}^{n+3/2} + V_{Fk}^{n+1/2})$$

or

$$I_k^{n+3/2} = F^{-1}\left(l\frac{\Delta z}{\Delta t} - A\frac{\Delta z}{2} + B\frac{\Delta z}{\sqrt{\pi \Delta t}} Z_0(0)\right) I_k^{n+1/2} \tag{5.154a}$$

$$- F^{-1} B\frac{\Delta z}{\sqrt{\pi \Delta t}} \sum_{m=1}^{n} (I_k^{n+3/2-m} - I_k^{n+1/2-m}) Z_0(m)$$

$$- \mathrm{F}^{-1}(\mathrm{V}_{k+1}^{n+1} - V_k^{n+1}) + F^{-1}\frac{\Delta z}{2}(V_{Fk}^{n+3/2} + V_{Fk}^{n+1/2})$$

for $k = 1, \ldots, NDZ$ where

$$F = \left(l\frac{\Delta z}{\Delta t} + A\frac{\Delta z}{2} + B\frac{\Delta z}{\sqrt{\pi \Delta t}} Z_0(0)\right) \tag{5.154b}$$

This replaces equation (5.120d) of the lossless case.

Unfortunately, this requires storage of all past values of the currents. A clever solution to this problem is presented in [21]. Prony's method can be used to

TABLE 5.1 Coefficients of the Prony Approximation of $Z_0(m)$

| $i$ | $a_i$ | $\alpha_i$ |
|---|---|---|
| 1 | 0.790 981 80E − 1 | −0.114 844 27E − 2 |
| 2 | 0.115 434 23E0 | −0.138 183 29E − 1 |
| 3 | 0.134 353 80E0 | −0.540 375 96E − 1 |
| 4 | 0.218 704 22E0 | −0.142 164 94E0 |
| 5 | 0.982 296 67E − 1 | −0.301 284 37E0 |
| 6 | 0.513 604 84E0 | −0.561 421 85E0 |
| 7 | −0.209 628 98E0 | −0.971 171 26E0 |
| 8 | 0.119 744 47E1 | −0.163 384 33E1 |
| 9 | 0.112 254 91E − 1 | −0.289 513 29E1 |
| 10 | −0.744 252 55E0 | −0.504 109 69E1 |

approximate $Z_0(m)$ as

$$Z_0(m) = \int_m^{(m+1)} \frac{1}{\sqrt{s}}\, ds \cong \sum_{i=1}^{N} a_i e^{m\alpha_i} \tag{5.155}$$

Kunz showed that a reasonable approximation can be obtained by using ten terms where the coefficients are given in Table 5.1 [21]. Substituting (5.155) into (5.154) yields

$$I_k^{n+3/2} = F^{-1}\left(1\frac{\Delta z}{\Delta t} - A\frac{\Delta z}{2} + B\frac{\Delta z}{\sqrt{\pi\Delta t}}Z_0(0)\right)I_k^{n+1/2} \tag{5.156a}$$

$$-F^{-1}B\frac{\Delta z}{\sqrt{\pi\Delta t}}\sum_{i=1}^{10}\Psi_i^n$$

$$-F^{-1}(V_{k+1}^{n+1} - V_k^{n+1}) + F^{-1}\frac{\Delta z}{2}(V_{Fk}^{n+3/2} + V_{Fk}^{n+1/2})$$

for $k = 1, \ldots, NDZ$ where

$$\Psi_i^n = a_i e^{\alpha_i}[I_k^{n+1/2} - I_k^{n-1/2}] + e^{\alpha_i}\Psi_i^{n-1} \tag{5.156b}$$

The $\Psi_i^n$ functions are updated via (5.156b) before evaluating (5.156a). Thus only one additional past value of current needs to be retained.

In the case of a multiconductor line a virtually identical development

provides

$$\mathbf{I}_k^{n+3/2} = \mathbf{F}^{-1}\left(\mathbf{L}\frac{\Delta z}{\Delta t} - \mathbf{A}\frac{\Delta z}{2} + \mathbf{B}\frac{\Delta z}{\sqrt{\pi\Delta t}}Z_0(0)\right)\mathbf{I}_k^{n+1/2} \tag{5.157a}$$

$$-\mathbf{F}^{-1}\mathbf{B}\frac{\Delta z}{\sqrt{\pi\Delta t}}\sum_{l=1}^{10}\Psi_l^n$$

$$-\mathbf{F}^{-1}(\mathbf{V}_{k+1}^{n+1} - \mathbf{V}_k^{n+1}) + \mathbf{F}^{-1}\frac{\Delta z}{2}(\mathbf{V}_{Fk}^{n+3/2} + \mathbf{V}_{Fk}^{n+1/2})$$

for $k = 1, \ldots, NDZ$ where

$$\Psi_l^n = a_l e^{\alpha_l}[\mathbf{I}_k^{n+1/2} - \mathbf{I}_k^{n-1/2}] + e^{\alpha_l}\Psi_l^{n-1} \tag{5.157b}$$

and

$$\mathbf{F} = \left(\mathbf{L}\frac{\Delta z}{\Delta t} + \mathbf{A}\frac{\Delta z}{2} + \mathbf{B}\frac{\Delta z}{\sqrt{\pi\Delta t}}Z_0(0)\right) \tag{5.157c}$$

This replaces equation (5.140d) of the lossless-line development. All other equations in (5.140) remain unchanged. This is implemented in the FORTRAN code **FDTDLOSS.FOR** described in Appendix A.

In order to compare the predictions of these models we will investigate a high-loss, two-conductor transmission line shown in Fig. 5.42. The dimensions are typical of thin-film circuits. Two conductors of rectangular cross section of width 20 μm and thickness 10 μm are separated by 20 μm and placed on one side of a silicon substrate ($\varepsilon_r = 12$) of thickness 100 μm. The total line length is 20 cm and is terminated at the near and far ends in 50 Ω resistors. The source is a ramp function rising to a level of 1 V with a risetime of 50 ps. The per-unit-length inductance and capacitance were computed using **PCBGAL.FOR** giving $l = 0.805\,969$ μH/m and $c = 88.248\,8$ pF/m. This gives a velocity of propagation in the lossless case of $v = 1.185\,73 \times 10^8$ m/s and a one-way time delay of $T = 1.686\,72$ ns which gives an effective dielectric constant of $\varepsilon_r' = 6.392\,5$ and a characteristic impedance of $Z_C = 95.566\,\Omega$. The per-unit-length dc resistance is computed as $A = r_{dc} = 1/(\sigma wt) = 86.207\,\Omega$/m. The break frequency where this transitions to the high-frequency resistance that varies as $\sqrt{f}$ is computed from (3.222) as $f_o = 393.06$ MHz. The factor $B$ is computed as described previously to be $B = 1/2(t + w)\sqrt{\mu/\sigma} = r_{dc}/\sqrt{\pi f_o} = 2.45323 \times 10^{-3}$. Figure 5.43(a) shows the comparison of the SPICE (lossless) predictions, the time-domain to frequency-domain transformation (TDFD), and the finite difference–time domain (FDTD) results for the near-end and far-end voltages. The time-domain to frequency-domain transformation modeled the source as a 10 MHz periodic trapezoidal waveform with 50% duty cycle and rise/fall times of 50 ps, and the code **TIMEFREQ.FOR** was used which uses the frequency-

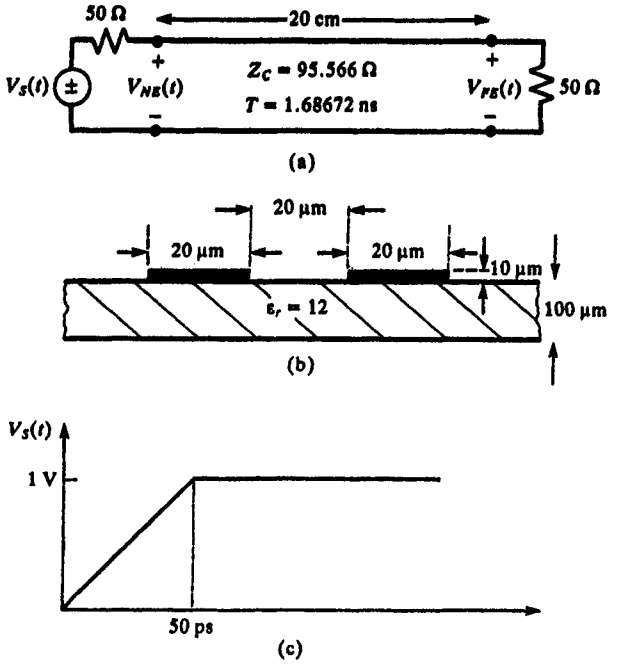


FIGURE 5.42 A lossy printed circuit board for illustration of numerical results: (a) line dimensions and terminations, (b) cross-sectional dimensions, and (c) representation of the open-circuit source-voltage waveform.

domain transfer function obtained from **MTL.FOR**. The high-frequency spectrum of this waveform rolls off at $-40$ dB/decade above $1/\pi\tau_r = 6.3662$ GHz so 2000 harmonics were used in the computation of the frequency response via the **MTL.FOR** code (giving an upper limit of 20 GHz). The spatial discretization for the FDTD results was chosen so that each cell was $\lambda/10$ at twice this break frequency giving $NDZ = 215$. The magic time step of $\Delta t = \Delta z/v$ for this spatial discretization and a total solution time of 10 ns is $NDT = 1275$.

The effect of line loss is evident and significant, but the time-domain to frequency-domain transformation method and the FDTD method give different results. This is due to the fact that the FDTD method simply adds the low-frequency dc resistance to the high-frequency impedance and models the total conductor impedances as

$$\begin{aligned} \hat{z}_i(\omega) &= A + B\sqrt{j\omega} \\ &= r_{dc} + r_{hf} + j\omega l_{i,hf} \\ &= r_{dc} + r_{dc}\sqrt{\frac{f}{f_o}}(1 + j) \end{aligned}$$

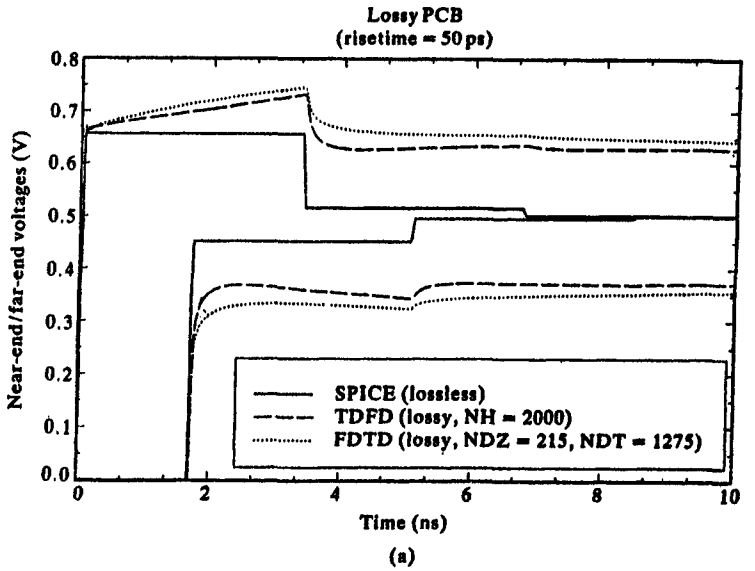


(a)

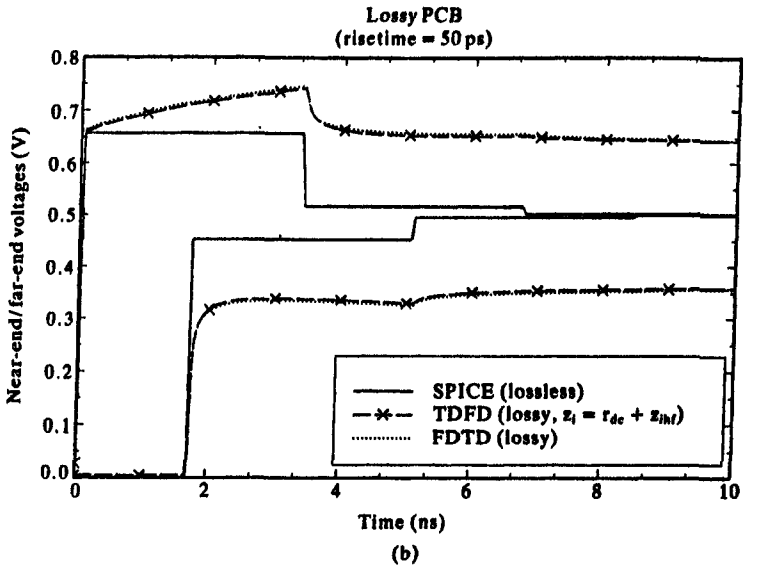


(b)

FIGURE 5.43 Comparison of the source and load voltages predicted by the SPICE (lossless) model, the time-domain to frequency-domain transformation (TDFD), and the finite difference–time-domain (FDTD) methods for the lossy PCB of Fig. 5.42: (a) complete models and (b) adding the dc and high-frequency impedance in the TDFD method to compare with the FDTD method.

The time-domain to frequency-domain method uses the frequency-domain transfer function computed with **MTL.FOR** which uses a frequency-selective model of the conductor impedances:

$$\hat{z}_i(\omega) = \begin{cases} r_{dc} + j\omega l_{i,dc} = r_{dc}(1 + jf/f_o) & f \le f_o \\ r_{hf} + j\omega l_{i,hf} = r_{dc}\sqrt{f/f_o}(1 + j) & f \ge f_o \end{cases}$$

At the break frequency, $f_o = 393.06$ MHz, the FDTD results are a factor of 2 larger than those of the frequency-selective TDFD method. The true value lies between these two values (see Figs. 3.52 and 3.53.) This break frequency lies in the $-20$ dB/decade region of the spectrum which begins at $1/\pi\tau = 6.366$ MHz and ends at $1/\pi\tau_r = 6.366$ GHz [A.3]. Thus we should expect a difference between the two model predictions. To verify that this is the case, we recompute the time-domain to frequency-domain transformation results wherein the low-frequency and high-frequency conductor impedances are added together in the frequency-domain transfer function as in the FDTD code rather than using a frequency-selective computation as described above. Figure 5.43(b) shows the results of this computation for the near-end and far-end voltages. These results confirm the hypothesis and show that the FDTD code gives virtually identical results to the time-domain to frequency-domain transformation method when the same equations are being solved.

In the applications of the FDTD technique to electromagnetic scattering problems, a surface-impedance boundary condition is frequently used. This condition essentially has a $\sqrt{f}$ frequency dependence and requires no constant resistance [16, 21]. Numerous solutions of the transmission-line equations for lossy lines include only the high-frequency, $\sqrt{f}$ impedance of the line conductors and ignore their dc, constant resistance. We have included this in the FDTD solution via the A term. The question is whether the dc resistance can be neglected and only the high-frequency $\sqrt{f}$ impedance used. Figure 5.44(a) shows the results of including only the dc resistance or only the high-frequency $\sqrt{f}$ impedance of the conductors. Including only the dc resistance gives the correct late-time dc level of the responses but the early-time results are not well predicted at the beginning of the transitions. Including only the high-frequency $\sqrt{f}$ impedance of the conductors does not predict the late-time dc levels. So it appears that both the dc and the high-frequency impedances must be included in the formulation. Figure 5.44(b) shows the comparison between the TDFD and FDTD models using only the dc resistance or only the high-frequency resistance. This again confirms the importance of including the dc resistance and additionally shows that the TDFD and FDTD models give virtually identical results when the same representations of the conductor impedances are used. The slight difference when $z_i = z_{i,hf}$ is probably due to approximation of the high-frequency convolution term in the FDTD code.

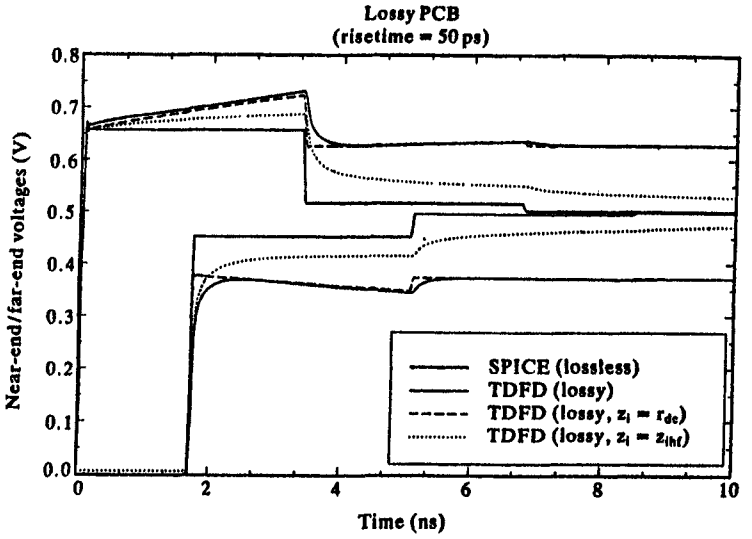


(a)

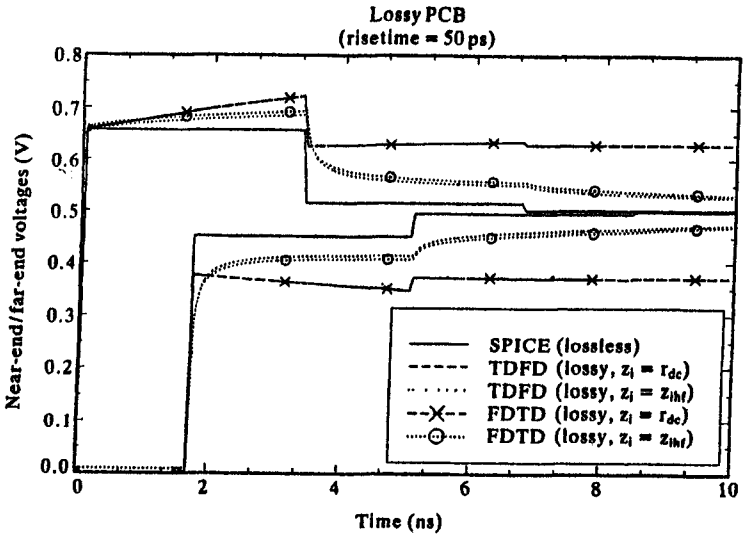


(b)

**FIGURE 5.44** Comparisons as in Fig. 5.43 with (a) the TDFD method using only the dc resistance and only the high-frequency impedance and (b) both methods using only the dc resistance or only the high-frequency impedance.

***5.3.1.4 Direct Solution via Inversion of the Laplace Transform*** The next solution method is the direct solution of the transmission-line equations given in (5.150). The propagation constant and characteristic impedance are

$$\gamma(s) = \sqrt{(A + B\sqrt{s} + sL)(G + sC)} \tag{5.158}$$

$$Z_C(s) = \sqrt{\frac{A + B\sqrt{s} + sL}{G + sC}} \tag{5.159}$$

We will omit the conductance term and assume *small losses.* The propagation constant and characteristic impedance require the square root of quantities involving the Laplace transform variable. This can be approximated by expanding the square root in a Taylor series and using the first two terms:

$$\sqrt{A + B\sqrt{s} + sL} = \sqrt{sL}\sqrt{1 + \frac{A + B\sqrt{s}}{sL}} \tag{5.160}$$

$$\approx \sqrt{sL}\left(1 + \frac{A + B\sqrt{s}}{2sL}\right)$$

which is valid for $|A + B\sqrt{s}| < |sL|$ which implies high frequencies and/or small losses. Under this approximation, the propagation constant and characteristic impedance become

$$\gamma(s) \approx s\sqrt{LC}\left(1 + \frac{A + B\sqrt{s}}{2sL}\right) \tag{5.161}$$

$$= \frac{s}{v_o} + \frac{A}{2Z_o} + \frac{B}{2Z_o}\sqrt{s}$$

$$Z_C(s) \approx \sqrt{\frac{L}{C}}\left(1 + \frac{A + B\sqrt{s}}{2sL}\right) \tag{5.162}$$

$$= Z_o + \frac{Av_o}{2s} + \frac{Bv_o}{2\sqrt{s}}$$

where the characteristic impedance and velocity of propagation for the lossless line are denoted by

$$Z_o = \sqrt{\frac{L}{C}} \tag{5.163}$$

$$v_o = \frac{1}{\sqrt{LC}} \tag{5.164}$$

The general solution to the transmission-line equations is of the form

$$V(z, s) = V^+(s)e^{-\gamma(s)z} + V^-(s)e^{\gamma(s)z} \tag{5.165a}$$

$$I(z, s) = \frac{1}{Z_C(s)}[V^+(s)e^{-\gamma(s)z} - V^-(s)e^{\gamma(s)z}] \tag{5.165b}$$

The direct solution and inversion of these expressions for general sources and loads is quite complicated. We will show the result for a unit-step-function source,

$$V_S(t) = V_o u(t) \Leftrightarrow \frac{V_o}{s} \tag{5.166}$$

zero source impedance, $Z_S(s) = 0$, and either an infinite or a matched line, $Z_L(s) = Z_C(s)$. In this case the general solution in (5.165) becomes

$$V(z, s) = \frac{V_o}{s} e^{-(A/2Z_o)z} e^{-(B/2Z_o)\sqrt{s}z} e^{-s(z/v_o)} \tag{5.167a}$$

$$I(z, s) = \frac{V_o}{Z_o\sqrt{s}\left(\sqrt{s} + \dfrac{Av_o}{2Z_o}\dfrac{1}{\sqrt{s}} + \dfrac{Bv_o}{2Z_o}\right)} e^{-(A/2Z_o)z} e^{-(B/2Z_o)\sqrt{s}z} e^{-s(z/v_o)} \tag{5.167b}$$

The term $e^{-A/2Z_o z}$ represents simple attenuation of the waveform amplitude, whereas the term $e^{-sz/v_o}$ represents time delay:

$$e^{-s(z/v_o)}F(s) \Leftrightarrow f(t - T_z) \tag{5.168}$$

where the time delay of the lossless line is denoted as $T_z = z/v_o$. The inverse Laplace transform of these results becomes [17]

$$V(z, t) = V_o e^{-(A/2Z_o)z} \operatorname{erfc}\left(\frac{B}{4Z_o}\frac{z}{(t - T_z)}\right)u(t - T_z) \tag{5.169a}$$

$$I(z, t) = \frac{V_o}{Z_o} e^{-(A/2Z_o)z} e^{(B^2v_o/4Z_o^2)z} e^{(Bv_o/2Z_o)^2(t - T_z)} \times \operatorname{erfc}\left(\frac{Bv_o}{2Z_o}\sqrt{t - T_z} + \frac{B}{4Z_o}\frac{z}{(t - T_z)}\right)u(t - T_z) \tag{5.169b}$$

and erfc denotes the tabulated complementary error function:

$$\operatorname{erfc}(x) = 1 - \frac{2}{\sqrt{\pi}} \int_0^x e^{-\tau^2}\, d\tau \tag{5.170}$$

$$= \frac{2}{\sqrt{\pi}} \int_x^\infty e^{-\tau^2}\, d\tau$$

The representation of $Z_1(s)$ in (5.143) characterizes the initial or early-time response when $A = 0$ and characterizes the final or late-time response when $B = 0$. So we would expect that ignoring the high-frequency resistance and internal inductance, $B = 0$, would yield early-time responses that are not realistic. This can be confirmed by setting $B = 0$ in (5.143) yielding

$$\gamma(s) = \frac{1}{v_o} \sqrt{s\left(s + \frac{A}{L}\right)} \tag{5.171}$$

$$Z(s) = Z_o \sqrt{1 + \frac{A}{sL}} \tag{5.172}$$

The current expression for the step response of a matched line becomes

$$I(z, s) = \frac{V_o}{Z_o s \sqrt{1 + \frac{A}{sL}}}\, e^{-(1/v_o)\sqrt{s(s + A/L)}z} \tag{5.173}$$

$$= \frac{V_o}{Z_o \sqrt{s\left(s + \frac{A}{L}\right)}}\, e^{-(1/v_o)\sqrt{s(s + A/L)}z}$$

The inverse Laplace transform is [17]

$$I(z, t) = \frac{V_o}{Z_o} e^{-(A/2L)t} I_0\left(\frac{A}{2L}\sqrt{t^2 - T_z^2}\right) u(t - T_z) \tag{5.174}$$

and $I_0(x)$ is the Bessel function of the first kind [17, 22]:

$$I_0(x) = 1 + \frac{x^2}{2^2} + \frac{x^4}{2^2 4^2} + \frac{x^6}{2^2 4^2 6^2} + \cdots \tag{5.175}$$

Consider a time immediately after the time delay to a point $z$, $t = T_z+$. The

result in (5.174) becomes

$$I(z, T_{z+}) = \frac{V_o}{Z_o} e^{-(A/2L)T_z} + u(T_{z+} - T_z) \tag{5.176}$$

since, according to (5.175), $I_0((A/2L)\sqrt{T_{z+}^2 - T_z^2}) \approx 1$. This result predicts a *step function change* in the line voltage at these points on the line but that is not realistic; the current should not change instantaneously. So evidently the high-frequency skin-effect impedance must be included in the time-domain result, $B \neq 0$, in order to generate realistic early-time responses.

Other responses such as the impulse response

$$V_S(t) = V_o \delta(t) \Leftrightarrow V_o \tag{5.177}$$

can be similarly obtained either by direct inversion of the Laplace transform or by differentiation of the step function result. For example, using the approximations in (5.161) and (5.162), the impulse response becomes

$$V(z, s) = V_o e^{-(A/2Z_o)z} e^{-(B/2Z_o)\sqrt{s}z} e^{-s(z/v_o)} \tag{5.178}$$

whose inverse Laplace transform is [17]

$$V(z, t) = V_o \frac{B}{4Z_o\sqrt{\pi}} \frac{z}{\sqrt{(t - T_z)^3}} e^{-(A/2Z_o)z} e^{-(B/4Z_o)^2(z^2/(t-T_z))} u(t - T_z) \tag{5.179}$$

The step response or the response to any other form of $V_S(t)$ can be obtained by convolution using this impulse response of the line [A.2].

Clearly, even for this simple case of a two-conductor line, the incorporation of losses is quite complicated and so are the results. Furthermore this direct solution has required the assumption of a matched or infinitely long line in order to provide simple transforms which are invertible. Thus we expect considerable solution difficulties for more practical cases of mismatched lines with nonlinear loads. The inversion of the Laplace transform result was also investigated in [23–25]. It is also possible to invert the Laplace transform numerically using the fast inversion of the Laplace transform (FILT) [26] sometimes known as the numerical inversion of the Laplace transform (NILT) [27, 28]. An extensive investigation of the properties of the Laplace transform of the response of a two-conductor lossy line is contained in [29].

*5.3.1.5 Time-Domain Characterization of the Line as a Two Port* The final solution method is to characterize the line as a two port representation *in the time domain.* Sources and loads (including nonlinear ones) can then be attached and the solution obtained. The advantage of this type of characterization is that the terminations are external to it and can be nonlinear.

The lumped-circuit iterative models such as the lumped-pi or lumped-T structures discussed previously are common examples of this notion. However, these models suffer from the requirement that many such cascaded sections that are electrically short at the highest frequency of interest are needed in order to correctly process the high-frequency spectral content of the input signal. An alternative to the requirement for a large number of cascaded sections is the following [30]. The chain parameter matrix of a lossy two-conductor line of length $\mathscr{L}$ is

$$\begin{bmatrix} V(\mathscr{L}, s) \\ I(\mathscr{L}, s) \end{bmatrix} = \begin{bmatrix} \cosh(\gamma(s)\mathscr{L}) & -Z_C(s)\sinh(\gamma(s)\mathscr{L}) \\ -\dfrac{1}{Z_C(s)}\sinh(\gamma(s)\mathscr{L}) & \cosh(\gamma(s)\mathscr{L}) \end{bmatrix} \begin{bmatrix} V(0, s) \\ I(0, s) \end{bmatrix} \tag{5.180}$$

Similarly, the admittance parameter representation is

$$\begin{bmatrix} \mathrm{I}(0, s) \\ -I(\mathscr{L}, s) \end{bmatrix} = \begin{bmatrix} Y_S(s) & -Y_M(s) \\ -Y_M(s) & Y_S(s) \end{bmatrix} \begin{bmatrix} V(0, s) \\ V(\mathscr{L}, s) \end{bmatrix} \tag{5.181a}$$

where the admittance parameters can be obtained from the chain parameter matrix as

$$Y_S(s) = \frac{1}{Z_C(s)\tanh(\gamma(s)\mathscr{L})} \tag{5.181b}$$

$$Y_M(s) = \frac{1}{Z_C(s)\sinh(\gamma(s)\mathscr{L})} \tag{5.181c}$$

This admittance representation can be synthesized as shown in Fig. 5.45(a). The task now becomes the synthesis of the networks that may be used to represent the elements

$$Y_S(s) - Y_M(s) = \frac{(\cosh(\gamma(s)\mathscr{L}) - 1)}{Z_C(s)\sinh(\gamma(s)\mathscr{L})} \tag{5.182a}$$

$$= \frac{1}{Z_C(s)}\tanh\left(\frac{\gamma(s)}{2}\mathscr{L}\right)$$

$$Y_M(s) = \frac{1}{Z_C(s)\sinh(\gamma(s)\mathscr{L})} \tag{5.182b}$$

First let us consider the frequency domain and ignore losses so that $\gamma\mathscr{L} = j\omega\mathscr{L}/v = j\beta\mathscr{L} = j2\pi\mathscr{L}/\lambda$ and $Z_C = \sqrt{l/c}$. The admittances of the elements

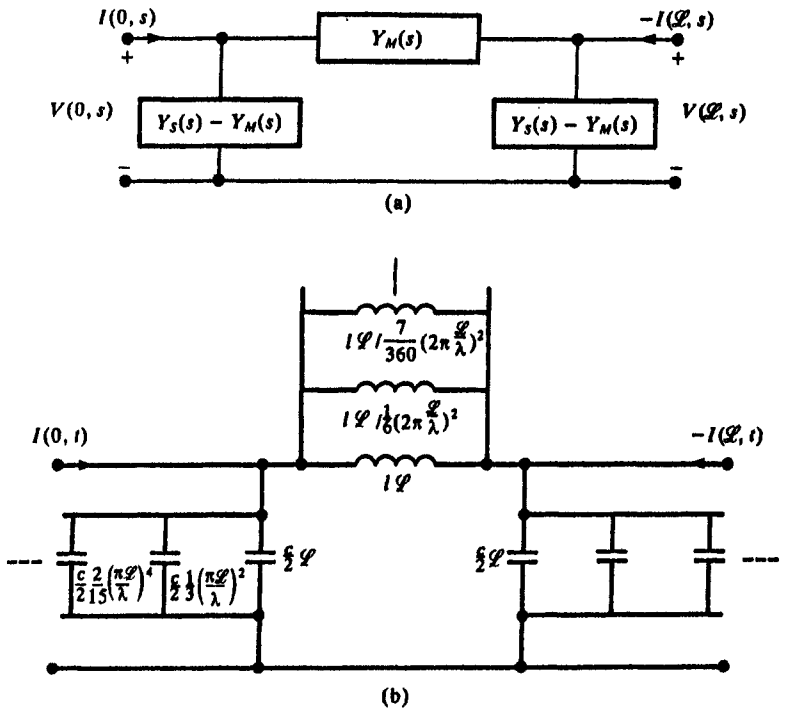


**FIGURE 5.45** Synthesis of equivalent circuits to represent the line's admittance parameters: (a) the admittance parameter reprsentation and (b) series representation of the individual admittance parameters for a lossless line.

become

$$Y_S(j\omega) - Y_M(j\omega) = j\frac{1}{Z_C}\tan\left(\pi\frac{\mathscr{L}}{\lambda}\right) \tag{5.183a}$$

$$Y_M(j\omega) = -j\frac{1}{Z_C \sin\left(2\pi\dfrac{\mathscr{L}}{\lambda}\right)} \tag{5.183b}$$

These trigonometric functions may be expanded in series form valid for $\mathscr{L} < \lambda/2$ using [22]

$$\tan x = x + \frac{x^3}{3!} + \frac{2}{15}x^5 + \cdots$$

$$\frac{1}{\sin x} = \frac{1}{x} + \frac{x}{6} + \frac{7}{360}x^3 + \cdots$$

This gives

$$Y_S(j\omega) - Y_M(j\omega) = j\omega \frac{c}{2} \mathscr{L}\left[1 + \frac{1}{3}\left(\frac{\pi\mathscr{L}}{\lambda}\right)^2 + \frac{2}{15}\left(\frac{\pi\mathscr{L}}{\lambda}\right)^4 + \cdots\right] \quad (5.184a)$$

$$Y_M(j\omega) = \frac{1}{j\omega l\mathscr{L}}\left[1 + \frac{1}{6}\left(2\pi\frac{\mathscr{L}}{\lambda}\right)^2 + \frac{7}{360}\left(2\pi\frac{\mathscr{L}}{\lambda}\right)^4 + \cdots\right] \quad (5.184b)$$

These admittance functions can be synthesized as cascades of admittances as illustrated in Fig. 5.45(b). Clearly, using the first terms gives the usual lumped-pi model that we have used previously. Although these expansions are only valid for lossless lines and line lengths less than one-half of one wavelength there are other expansions of the trigonometric functions that extend this region of validity and, in addition, accommodate lossy lines [30]. A number of other methods also seek to obtain expansions using infinite-ladder-type networks to represent the appropriate impedance/admittance functions [31].

Another frequently-used model is the extension to lossy lines of the method of characteristics, Branin's method, discussed previously for lossless lines [27, 28, 32–34]. These methods frequently assume only dc resistance and ignore skin-effect $\sqrt{f}$ dependence. The chain parameter matrix in (5.180) is inverted to yield

$$\begin{bmatrix} V(0,s) \\ I(0,s) \end{bmatrix} = \begin{bmatrix} \cosh\theta(s) & Z_C(s)\sinh\theta(s) \\ \dfrac{1}{Z_C(s)}\sinh\theta(s) & \cosh\theta(s) \end{bmatrix} \begin{bmatrix} V(\mathscr{L},s) \\ I(\mathscr{L},s) \end{bmatrix} \quad (5.185a)$$

where

$$\theta(s) = \gamma(s)\mathscr{L} = \sqrt{(r+sl)(g+sc)}\,\mathscr{L} \quad (5.185b)$$

$$Z_C(s) = \sqrt{\frac{r+sl}{g+sc}} \quad (5.185c)$$

These equations can be converted into the following equations which are similar to the method of characteristics for lossless lines:

$$V(0,s) - Z_C(s)I(0,s) = e^{-\theta(s)}[V(\mathscr{L},s) - Z_C(s)I(\mathscr{L},s)] \quad (5.186a)$$

$$V(\mathscr{L},s) + Z_C(s)I(\mathscr{L},s) = e^{-\theta(s)}[V(0,s) + Z_C(s)I(0,s)] \quad (5.186b)$$

These relations may be represented as shown in Fig. 5.46 where

$$E_0(s) = e^{-\theta(s)}[2V(\mathscr{L},s) - E_{\mathscr{L}}(s)] \quad (5.187a)$$

$$E_{\mathscr{L}}(s) = e^{-\theta(s)}[2V(0,s) - E_0(s)] \quad (5.187b)$$

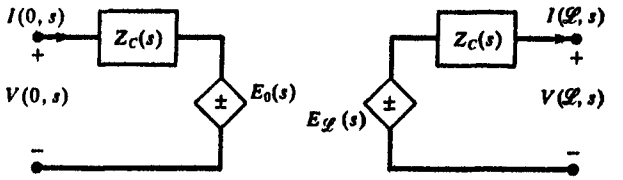


FIGURE 5.46 Representation of a lossy, two-conductor line with the generalized method of characteristics.

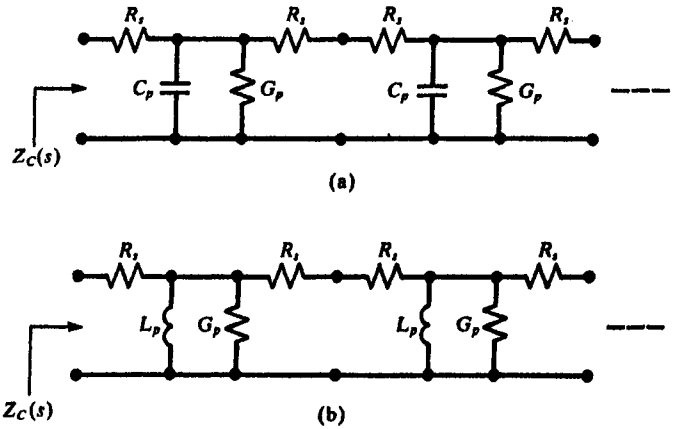


FIGURE 5.47 Ladder representations of the characteristic impedances of a lossy line.

Therefore, the lossy line can be simulated as in Fig. 5.46 if we can synthesize appropriate representations for $Z_C(s)$ and $e^{-\theta(s)}$. For example, the characteristic impedance for lossy lines, $Z_C(s) = \sqrt{(r + sl)/(g + sc)}$, can be expanded in the form of a ladder network consisting of an infinite cascade of symmetrical T networks consisting of series and parallel impedances shown in Fig. 5.47 using the Padé approximation method [27, 32]. Recall that this expansion is valid for constant $r$ and $g$, i.e., the skin effect is ignored. Chang showed that a small number of these structures (approximately four) will simulate the characteristic impedance quite well. The network shown in Fig. 5.47(a) is used if the characteristic impedance is "capacitive" meaning $c > gl/r$, and the network shown in Fig. 5.47(b) is used if the characteristic impedance is "inductive" meaning $l > rc/g$. The elements are given in Table 5.2 [32].

A useful way of interpreting the exponential propagation function is by determining the unit-impulse response that it represents and using *convolution* in conjunction with (5.187). The impulse response of the propagation function is

$$H(s) = e^{-\theta(s)} = e^{-\sqrt{lc}\ell\sqrt{s^2 + (rc + lg/lc)s + (rg/lc)}} \tag{5.188}$$

**TABLE 5.2 Elements of the Circuits of Fig. 5.47**

| Capacitive $Z_C(s)$ $p = rc/gl > 1$ | Inductive $Z_C(s)$ $p = rc/gl < 1$ |
|---|---|
| $R_s = \sqrt{l/c}$ | $R_s = \sqrt{r/g}$ |
| $G_p = \alpha g\mathscr{L}$ | $G_p = \beta g\mathscr{L}$ |
| $C_p = \alpha c\mathscr{L}$ | $L_p = \gamma l\mathscr{L}$ |
| $\alpha = 2/[(p-1)\sqrt{lcg}\mathscr{L}]$ | $\beta = 2p/[(1-p)\sqrt{rg}\mathscr{L}]$ |
| | $\gamma = (1-p)/(2\sqrt{rg}\mathscr{L})$ |

The inverse Laplace transform is [27]

$$h(t) = e^{-aT}\delta(t-T) + e^{-aT}\frac{bT}{\sqrt{t^2-T^2}}I_1(b\sqrt{t^2-T^2})u(t-T) \quad (5.189a)$$

where

$$a = \frac{rc+gl}{2lc} \quad (5.189b)$$

$$b = \frac{|lg-rc|}{2lc} \quad (5.189c)$$

$T = \mathscr{L}/v$ is the total one-way line delay, and $I_1$ is the modified Bessel function of the first kind. A similar direct convolution is obtained in [35]. A first-order approximation to the propagation function can also be obtained using the small loss approximation of the first two terms in a Taylor series expansion given in (5.161):

$$e^{-\theta(s)} \cong e^{-A\mathscr{L}/2Z_0}e^{-(B\mathscr{L}/2Z_0)\sqrt{s}}e^{-sT} \quad (5.190)$$

whose inverse Laplace transform is [17]

$$h(t) = \frac{B}{4Z_0\sqrt{\pi}}\frac{\mathscr{L}}{\sqrt{(t-T)^3}}e^{-(A\mathscr{L}/2Z_0)}e^{-(B/4Z_0)^2\mathscr{L}^2/(t-T)}u(t-T) \quad (5.191)$$

In either case the outputs of the controlled sources in Fig. 5.46 are obtained from (5.187) by convolution using these impulse responses as

$$E_0(t) = \int_0^t h(t-\tau)[2V(\mathscr{L},\tau) - E_{\mathscr{L}}(\tau)]\,d\tau \quad (5.192a)$$

$$E_{\mathscr{L}}(t) = \int_0^t h(y-\tau)[2V(0,\tau) - E_0(t)]\,d\tau \quad (5.192b)$$

### 5.3.2 Multiconductor Lines

Many of the techniques for two-conductor lines are adaptable to MTL's. The prominent ones are the lumped-circuit iterative approximate structures such as the lumped-pi and lumped-T structures, the time-domain to frequency-domain transformation, and the finite difference–time domain (FDTD) technique (equations (5.140) with equation (5.157) replacing (5.140d)). The FORTRAN programs **SPICELPI.FOR, TIMEFREQ.FOR** and **FDTDLOSS.FOR** are written to handle these cases for MTL's. With the exception of these techniques, the time-domain solution of the MTL equations for lossy lines is generally a formidable task. In this section we discuss some of the remaining methods for lossy MTL's.

The MTL equations can be easily decoupled via similarity transformations in the case of *lossless* lines as demonstrated previously. In the general case of lossy lines this is not possible except for certain special cases that exhibit structural symmetry. In attempting to decouple the MTL equations for lossy lines we again convert to *modal* quantities with similarity transformations:

$$\mathbf{V}(z, s) = \mathbf{T}_V \mathbf{V}_m(z, s) \tag{5.193a}$$

$$\mathbf{I}(z, s) = \mathbf{T}_I \mathbf{I}_m(z, s) \tag{5.193b}$$

where we have denoted the line voltages and currents as their Laplace-transformed variables to simplify the equations with respect to the time variable. Substituting these into the complete MTL equations yields

$$\frac{d}{dz}\mathbf{V}_m(z, s) = \mathbf{T}_V^{-1}\mathbf{R}(s)\mathbf{T}_I\mathbf{I}_m(z, s) + s\mathbf{T}_V^{-1}(\mathbf{L}_i(s) + \mathbf{L}_e)\mathbf{T}_I\mathbf{I}_m(z, s) \tag{5.194a}$$

$$\frac{d}{dz}\mathbf{I}_m(z, s) = \mathbf{T}_I^{-1}\mathbf{G}(s)\mathbf{T}_V\mathbf{V}_m(z, s) + s\mathbf{T}_I^{-1}\mathbf{C}\mathbf{T}_V\mathbf{V}_m(z, s) \tag{5.194b}$$

Observe that the resistance matrix, $\mathbf{R}(s)$, and the internal inductance matrix, $\mathbf{L}_i(s)$, are each shown as being functions of $s$ which will be the case unless skin-effect losses are ignored and only dc resistance and internal inductance are considered. Similarly, the conductance matrix, $\mathbf{G}(s)$, is, in general, a function of $s$. The intention is to find the $n \times n$ transformation matrices $\mathbf{T}_V$ and $\mathbf{T}_I$ such that these modal equations are *uncoupled*. If this were possible, we could simulate the modes with uncoupled, two-conductor lossy *modal* lines using the previous results for two-conductor lines from Fig. 5.46. The transformations from mode to actual line currents and voltages via (5.193) could be implemented in the same manner as for lossless lines using controlled sources as illustrated in Fig. 5.48. Recall also that $\mathbf{R}$ and a portion of $\mathbf{L}$, the internal inductance contribution, contain frequency-dependent parameters corresponding to the internal impedances of the conductors. So, in general the transformation matrices will be functions of $s$. However, it is desirable that the transformations

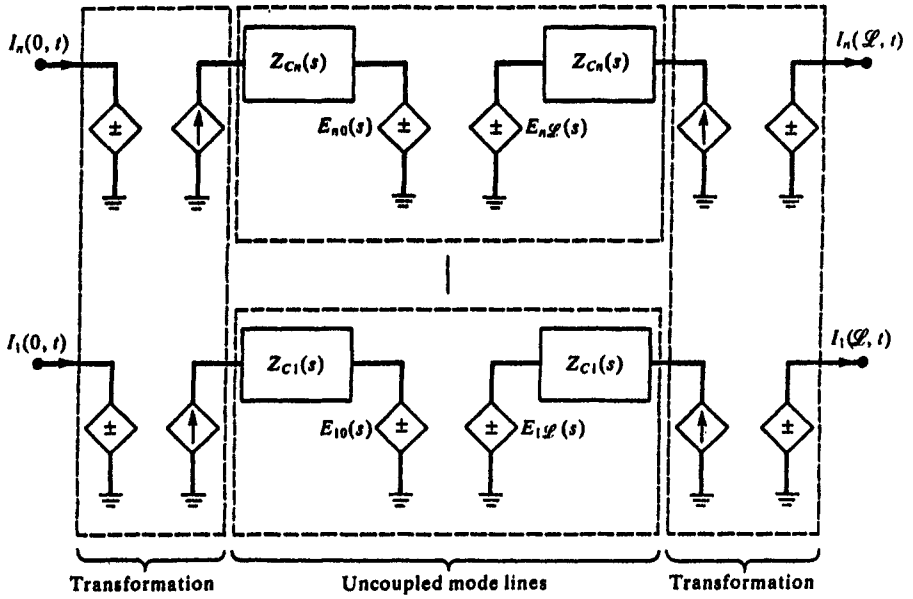


FIGURE 5.48 Representation of a lossy MTL via the generalized method of characteristics in terms of uncoupled modes and lossy two-conductor mode lines.

be independent of $s$ so that the controlled-source parameters are constants. Controlled sources that are functions of $s$ which represent the general case were implemented in [31]. This general goal of decoupling the MTL equations is often referred to as the generalized method of characteristics [36–42] although it has not been fully realized because of the inability to completely decouple the lossy-line MTL equations.

The procedure for accomplishing this is more easily observed by writing the MTL equations as uncoupled, second-order equations as shown in equation (2.31):

$$\frac{d^2}{dz^2}\mathbf{V}_m(z, s) = \mathbf{T}_V^{-1}[\mathbf{RG}]\mathbf{T}_V\mathbf{V}_m(z, s) + s\mathbf{T}_V^{-1}[\mathbf{RC} + \mathbf{LG}]\mathbf{T}_V\mathbf{V}_m(z, s) \quad (5.195a)$$

$$+ s^2\mathbf{T}_V^{-1}[\mathbf{LC}]\mathbf{T}_V\mathbf{V}_m(z, s)$$

$$\frac{d^2}{dz^2}\mathbf{I}_m(z, s) = \mathbf{T}_I^{-1}[\mathbf{GR}]\mathbf{T}_I\mathbf{I}_m(z, s) + s\mathbf{T}_I^{-1}[\mathbf{GL} + \mathbf{CR}]\mathbf{T}_I\mathbf{I}_m(z, s) \quad (5.195b)$$

$$+ s^2\mathbf{T}_I^{-1}[\mathbf{CL}]\mathbf{T}_I\mathbf{I}_m(z, s)$$

Because the per-unit-length parameter matrices are symmetric it suffices to

decouple (5.195b) and let

$$\mathbf{T} = \mathbf{T}_I \tag{5.196a}$$

$$\mathbf{T}^t = \mathbf{T}_V^{-1} \tag{5.196b}$$

So we must find an $n \times n$ matrix $\mathbf{T}$ which simultaneously diagonalizes the following three matrices:

$$\mathbf{T}^{-1}(\mathbf{GR})\mathbf{T} = \Lambda_1 \tag{5.197a}$$

$$\mathbf{T}^{-1}(\mathbf{GL} + \mathbf{CR})\mathbf{T} = \Lambda_2 \tag{5.197b}$$

$$\mathbf{T}^{-1}(\mathbf{CL})\mathbf{T} = \Lambda_3 \tag{5.197c}$$

We observed previously that it is possible to obtain a transformation $\mathbf{T}$ that will diagonalize the product of two real, symmetric, positive definite matrices as are $\mathbf{C}$ and $\mathbf{L}$. Clearly it is too much to expect to be able to find one transformation $\mathbf{T}$ that will simultaneously diagonalize all three matrices in (5.197) with one transformation and, furthermore, to have that transformation be independent of $s$. In order to show the special cases which can be decoupled with one constant transformation, $\mathbf{T}$, suppose that we assume a perfect medium, $\mathbf{G} = \mathbf{0}$. Now we must diagonalize two matrices:

$$\mathbf{T}^{-1}(\mathbf{CR})\mathbf{T} = \Lambda_2 \tag{5.198a}$$

$$\mathbf{T}^{-1}(\mathbf{CL})\mathbf{T} = \Lambda_3 \tag{5.198b}$$

There are certain special cases where a constant transformation, $\mathbf{T}$, can be found that simultaneously diagonalizes both matrices in (5.198). These are:

1. $(n + 1)$ identical conductors ignoring loss in the reference conductor.
2. $(n + 1)$ identical conductors in homogeneous media.

The key here is the observation that for $n$ identical conductors, the per-unit-length resistance matrix is of the form

$$\mathbf{R} = \begin{bmatrix} r + r_0 & r_0 & r_0 & r_0 \\ r_0 & r + r_0 & r_0 & r_0 \\ r_0 & r_0 & r + r_0 & r_0 \\ r_0 & r_0 & r_0 & r + r_0 \end{bmatrix} \tag{5.199}$$

$$= r\mathbf{1}_n + r_0\mathbf{U}_n$$

where $\mathbf{1}_n$ is the $n \times n$ identity matrix with ones on the main diagonal and zeros elsewhere and $\mathbf{U}_n$ is the $n \times n$ unit matrix with ones in all positions. In the first

case, $\mathbf{R} = r\mathbf{1}_n$ and

$$[r(s) + sl_i(s)]\mathbf{T}^{-1}(\mathbf{C})\mathbf{T} = \mathbf{\Lambda}_2 \tag{5.200a}$$

$$\mathbf{T}^{-1}(\mathbf{CL})\mathbf{T} = \mathbf{\Lambda}_3 \tag{5.200b}$$

where we have extracted the internal inductances so that $\mathbf{L} = \mathbf{L}_e$. By the procedure given in Section 5.2.1.2 this is always possible (see (5.72)). In the next case we have the fundamental identity for a homogeneous medium, $\mathbf{CL} = 1/v^2\mathbf{1}_n$, so that

$$[r(s) + sl_i(s)]\mathbf{T}^{-1}[\mathbf{C}(\mathbf{1}_n + \mathbf{U}_n)]\mathbf{T} = \mathbf{\Lambda}_2 \tag{5.201a}$$

$$\frac{1}{v^2}\mathbf{T}^{-1}[\mathbf{1}_n]\mathbf{T} = \frac{1}{v^2}\mathbf{1}_n = \mathbf{\Lambda}_3 \tag{5.201b}$$

But $\mathbf{C}$ and $(\mathbf{1}_n + \mathbf{U}_n)$ are both real, symmetric and positive definite so that diagonalization of (5.201a) is assured. The above has demonstrated those special cases that can be decoupled. There are other apparent cases such as the assumption that only nearest-neighbor coupling occurs so that $\mathbf{C}$ and $\mathbf{L}$ are tridiagonal Toeplitz matrices [42]. But this requires identical conductors and neglecting loss in the reference conductor also in order to work so we may as well diagonalize the full $\mathbf{C}$ and $\mathbf{L}$ as in (5.200) and not assume only nearest-neighbor coupling.

When neither of the above special cases of identical conductors exist, the MTL equations in terms of modes in (5.194) cannot be decoupled. However, they can be placed in the form of ordinary differential equations (which are coupled) and numerically integrated. For example, suppose we assume $\mathbf{R}$ and $\mathbf{G}$ are constant (omit skin-effect losses) and neglect the internal inductance, $\mathbf{L}_i(s) = \mathbf{0}$. If we choose a modal transformation that diagonalizes the inductance and capacitance matrices, then the modal equations become

$$\frac{d}{dz}\mathbf{V}_m(z, s) = \mathbf{R}_m\mathbf{I}_m(z, s) + s\mathbf{L}_m\mathbf{I}_m(z, s) \tag{5.202a}$$

$$\frac{d}{dz}\mathbf{I}_m(z, s) = \mathbf{G}_m\mathbf{V}_m(z, s) + s\mathbf{C}_m\mathbf{V}_m(z, s) \tag{5.202b}$$

where

$$\mathbf{T}_V^{-1}\mathbf{L}_e\mathbf{T}_I = \mathbf{L}_m \quad \text{(diagonal)} \tag{5.203a}$$

$$\mathbf{T}_I^{-1}\mathbf{C}\mathbf{T}_V = \mathbf{C}_m \quad \text{(diagonal)} \tag{5.203b}$$

$$\mathbf{T}_V^{-1}\mathbf{R}\mathbf{T}_I = \mathbf{R}_m \quad \text{(not diagonal)} \tag{5.203c}$$

$$\mathbf{T}_I^{-1}\mathbf{G}\mathbf{T}_V = \mathbf{G}_m \quad \text{(not diagonal)} \tag{5.203d}$$

Note that only $\mathbf{L}$ and $\mathbf{C}$ can be diagonalized so that the modal equations in

(5.202) are not uncoupled. Tripathi in [36] places these in the form of ordinary differential equations via the generalized method of characteristics in the following manner. Define the modal characteristics as

$$d\mathbf{V}_m = dz\frac{\partial}{\partial z}\mathbf{V}_m + dt\frac{\partial}{\partial t}\mathbf{V}_m \tag{5.204a}$$

$$d\mathbf{I}_m = dz\frac{\partial}{\partial z}\mathbf{I}_m + dt\frac{\partial}{\partial t}\mathbf{I}_m \tag{5.204b}$$

where $dz$ is a diagonal matrix containing the derivatives of the $n$ axes of the $z$–$t$ plane defining the characteristic curves. Substituting (5.202) into (5.204) yields

$$dt\mathbf{1}_n - dz(\mathbf{L}_m\mathbf{C}_m)^{1/2} = 0 \tag{5.205a}$$

$$d\mathbf{V}_m + \mathbf{Z}_{Cm}\,d\mathbf{I}_m + dz(\mathbf{Z}_{Cm}\mathbf{G}_m\mathbf{V}_m + \mathbf{R}_m\mathbf{I}_m) = 0 \tag{5.205b}$$

$$dt\mathbf{1}_n + dz(\mathbf{L}_m\mathbf{C}_m)^{1/2} = 0 \tag{5.205c}$$

$$d\mathbf{V}_m - \mathbf{Z}_{Cm}\,d\mathbf{I}_m + dz(-\mathbf{Z}_{Cm}\mathbf{G}_m\mathbf{V}_m + \mathbf{R}_m\mathbf{I}_m) = 0 \tag{5.205d}$$

where $\mathbf{1}_n$ is the $n \times n$ identity matrix and $\mathbf{Z}_{Cm}$ is the $n \times n$ diagonal modal characteristic impedance matrix with entries $[\mathbf{Z}_{Cm}]_{ii} = \sqrt{[\mathbf{L}_m]_{ii}/[\mathbf{C}_m]_{ii}}$ on the main diagonal. Equation (5.205a) defines the $n$ families of characteristic curves along which (5.205b) holds, and (5.205c) defines the $n$ families of characteristic curves along which (5.205d) holds. The ordinary differential equations in (5.205) are solved numerically by approximating the time variables as $\Delta t$ and approximating the derivatives as first-order differences. The method was extended to include frequency-dependent skin-effect losses of the conductors and frequency-dependent losses in the medium in [37]. This technique follows the usual method of characteristics for two-conductor lines with the added complexity of coupled equations.

Another interesting technique that shows promise is the asymptotic waveform evaluation (AWE) method [43, 44]. It seeks to expand the Laplace-transformed voltages and currents in power series in the Laplace transform variable $s$ or moments. By matching matrix coefficients of corresponding powers of $s$ the MTL equations are transformed into a series of differential equations each of which can be diagonalized, and the various voltages and currents in the series expansions are solved for recursively. The method is currently restricted to constant **R**, i.e., the skin effect is not included.

### 5.3.3 Computed Results

The computed results are for the ribbon cable (shown in cross section in Fig. 4.14) and the PCB (shown in cross section in Fig. 4.17) with 50 Ω loads shown in Fig. 5.29. We will show the predictions of the lossless SPICE model, the

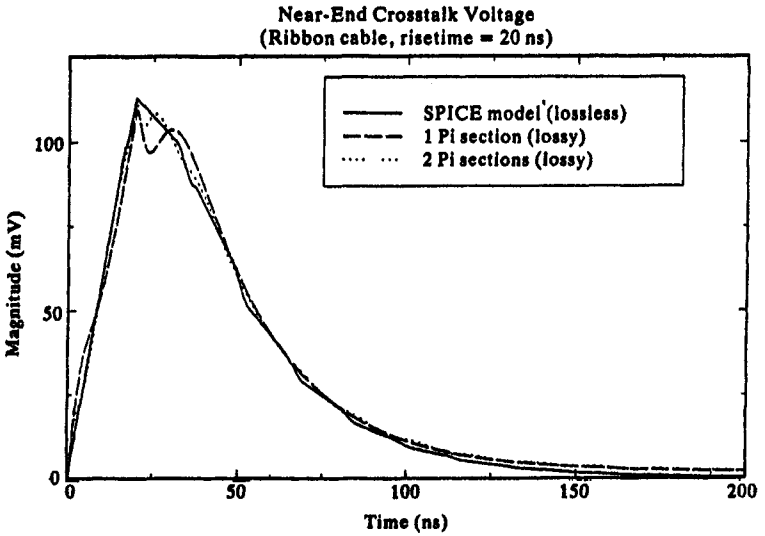


**FIGURE 5.49** Comparison of the time-domain response of the near-end crosstalk of the ribbon cable of Fig. 4.14 determined via the SPICE model (lossless) and the lumped-pi model (dc losses included) using one and two sections to represent the line for a pulse risetime of 20 ns.

lumped-pi approximate model, the time-domain to frequency-domain transformation method (TDFD), and the finite difference–time domain (FDTD) methods for the lossy lines.

*5.3.3.1 Ribbon Cable* Figure 5.49 shows the comparison of the SPICE (lossless) model and the predictions of the lumped-pi iterative model using one and two sections for the 2 m ribbon cable and a rise/fall time of the pulse of 20 ns. Figure 5.50 shows the comparison of the SPICE (lossless) model, the time-domain to frequency-domain transformation (using 100 harmonics of the 1 MHz pulse train), and the FDTD model (using 2 divisions of the line and 50 divisions of the time axis). All models give approximately the same results, and the losses appear to be inconsequential for this configuration and rise/fall time. Figure 5.51 shows the comparison of the lossless SPICE model, the time-domain to frequency-domain transformation (using 1000 harmonics of the 1 MHz pulse train) and the FDTD model (using 25 divisions of the line and 750 divisions of the time axis) for a pulse risetime of 1 ns. The losses give a dc offset during the period when the pulse is in its 1 V stable state which is referred to as common-impedance coupling and is due to the resistance of the reference conductor.

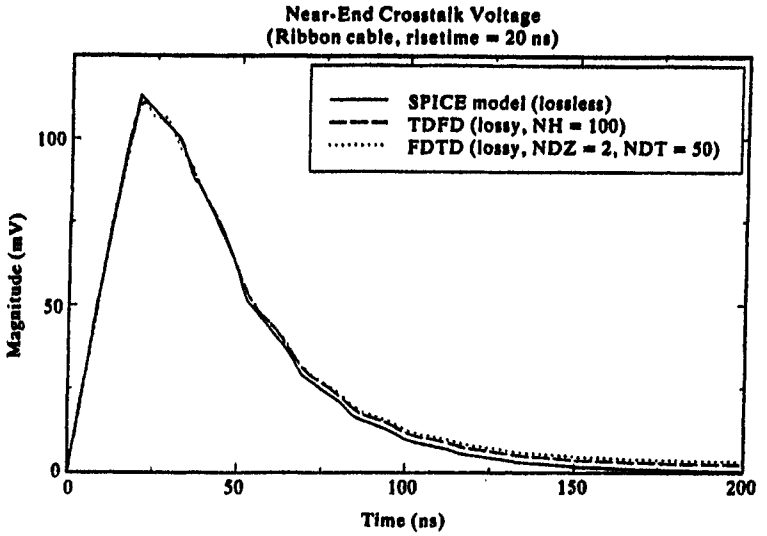


**FIGURE 5.50** Comparison of the time-domain response of the near-end crosstalk of the ribbon cable of Fig. 4.14 determined via the SPICE model (lossless), the time-domain to frequency-domain method (TDFD) (with skin-effect losses), and the finite difference–time-domain (FDTD) method (with skin-effect losses) for a pulse risetime of 20 ns.

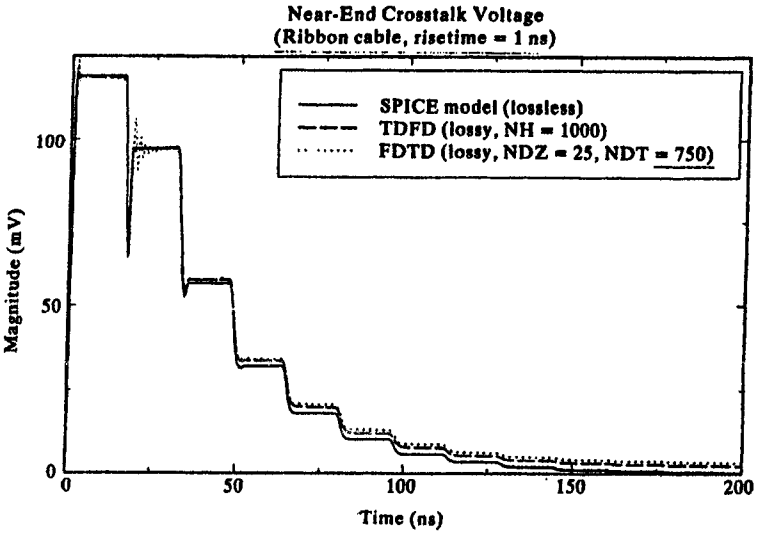


**FIGURE 5.51** Comparison of the time-domain response of the near-end crosstalk of the ribbon cable of Fig. 4.14 determined via the SPICE model (lossless), the time-domain to frequency-domain (TDFD) method (with skin-effect losses), and the finite difference–time-domain method (FDTD) (with skin-effect losses) for a pulse risetime of 1 ns.

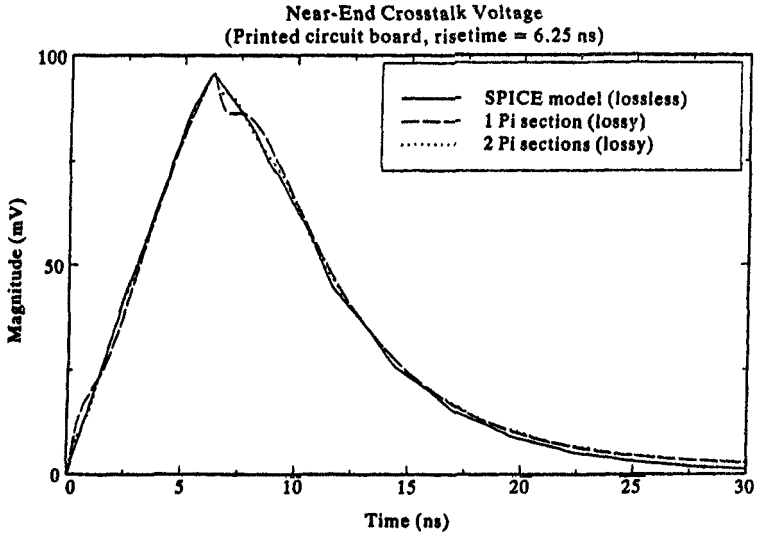


**FIGURE 5.52** Comparison of the time-domain response of the near-end crosstalk of the printed circuit board of Fig. 4.17 determined via the SPICE model (lossless) and the lumped-pi model (dc losses included) using only one and two sections to represent the line for a pulse risetime of 6.25 ns.

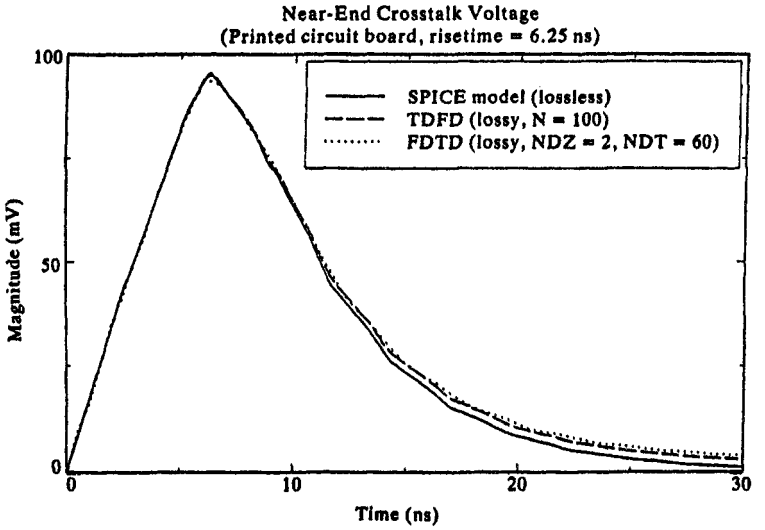


**FIGURE 5.53** Comparison of the time-domain response of the near-end crosstalk of the printed circuit board of Fig. 4.17 determined via the SPICE model (lossless), the time-domain to frequency-domain (TDFD) method (with skin-effect losses), and the finite difference–time-domain method (FDTD) (with skin-effect losses) for a pulse risetime of 6.25 ns.

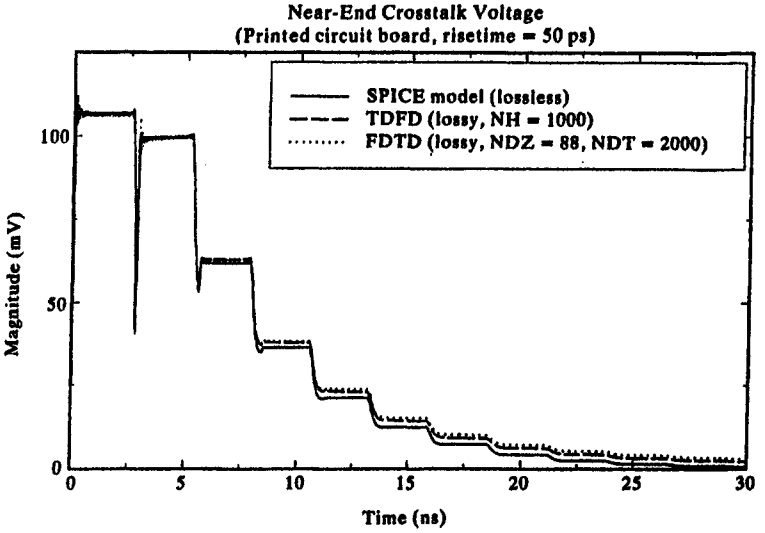


**FIGURE 5.54** Comparison of the time-domain response of the near-end crosstalk of the printed circuit board of Fig. 4.17 determined via the SPICE model (lossless), the time-domain to frequency-domain (TDFD) method (with skin-effect losses), and the finite difference–time-domain method (FDTD) (with skin-effect losses) for a pulse risetime of 50 ps.

*5.3.3.2 Printed Circuit Board* Figure 5.52 shows the comparison of the SPICE (lossless) model and the predictions of the lumped-pi iterative model using one and two sections for the 25.4 cm PCB and a pulse rise/fall time of 6.25 ns. Figure 5.53 shows the comparison of the SPICE (lossless) model, the time-domain to frequency-domain transformation (using 100 harmonics of the 10 MHz pulse train), and the FDTD model (using 2 divisions of the line and 60 divisions of the time axis). All models again give approximately the same results. Figure 5.54 shows the comparisons of the lossless SPICE model, the time-domain to frequency-domain transformation (using 1000 harmonics of the 10 MHz pulse train), and the FDTD model (using 88 divisions of the line and 2000 divisions of the time axis) for a pulse rise-time of 50 ps. Again the losses are not significant for this configuration except for the slight dc offset caused by common-impedance coupling.

## REFERENCES

[1] F.H. Branin, Jr., "Transient Analysis of Lossless Transmission Lines," *Proc. IEEE*, **55**, 2012–2013, 1967.

[2] L. Bergeron, *Water Hammer in Hydraulics and Wave Surges in Electricity*, John Wiley, NY, 1961.

[3] W. Frey and P. Althammer, "The Calculation of Electromagnetic Transients on Lines by Means of a Digital Computer," *The Brown Boveri Review*, **48**, 344–355 (1961).

[4] R.S. Singleton, "No Need to Juggle Equations to Find Reflection—Just Draw Three Lines," *Electronics*, **41**, 93–99 (1968).

[5] A. Ralston, *A First Course in Numerical Analysis*, McGraw-Hill, NY, 1965.

[6] H. Amemiya, "Time Domain Analysis of Multiple Parallel Transmission Lines," *RCA Review*, **28**, 241–276 (1967).

[7] F.Y. Chang, "Transient Analysis of Lossless Coupled Transmission Lines in Inhomogeneous Dielectric Media," *IEEE Trans. on Microwave Theory and Techniques*, **MTT-18**, 616–626 (1970).

[8] C.W. Ho, "Theory and Computer-aided Analysis of Lossless Transmission Lines," *IBM J. Research and Development*, **17**, 249–255 (1973).

[9] K.D. Marx, "Propagation Modes, Equivalent Circuits, and Characteristic Terminations for Multiconductor Transmission Lines with Inhomogeneous Dielectrics," *IEEE Trans. on Microwave Theory and Techniques*, **MTT-21**, 450–457 (1973).

[10] V.K. Tripathi and J.B. Rettig, "A SPICE Model for Multiple Coupled Microstrips and Other Transmission Lines," *IEEE Trans. on Microwave Theory and Techniques*, **MTT-33**, 1513–1518 (1985).

[11] A.K. Agrawal, H.J. Price, and S.H. Gurbaxani, "Transient Response of Multiconductor Transmission Lines Excited by a Nonuniform Electromagnetic Field," *IEEE Trans. on Electromagnetic Compatibility*, **EMC-22**, 119–129 (1980).

[12] D.F. Higgins, "Calculating Transmission Line Transients on Personal Computers," *Proc. IEEE International Symposium on Electromagnetic Compatibility*, August 25–27, 1987, Atlanta, GA.

[13] A.R. Djordjevic, T.S. Sarkar, and R.F. Harrington, "Time-Domain Response of Multiconductor Transmission Lines," *Proc. IEEE*, **75**, 743–764 (1987).

[14] R.L. Wiggington and N.S. Nahman, "Transient Analysis of Coaxial Cables Considering Skin Effect," *Proc. IRE*, **45**, 166–174 (1957).

[15] N.S. Nahman and D.R. Holt, "Transient Analysis of Coaxial Cables Using the Skin Effect Approximation $A + B\sqrt{s}$," *IEEE Trans. on Circuit Theory*, **19**, 443–451 (1972).

[16] F.M. Tesche, "On the Inclusion of Losses in Time-Domain Solutions of Electromagnetic Interaction Problems," *IEEE Trans. on Electromagnetic Compatibility*, **32**, 1–4 (1990).

[17] R.V. Churchill, *Operational Mathematics*, 2d ed., McGraw-Hill, NY, 1958.

[18] C. Yen, Z. Fazarinc, and R.L. Wheeler, "Time-Domain Skin-Effect Model for Transient Analysis of Lossy Transmission Lines," *Proc. IEEE*, **70**, 750–757 (1982).

[19] T. Vu Dinh, B. Cabon, and J. Chilo, "Time Domain Analysis of Skin Effect on Lossy Interconnections," *Electronics Lett.*, **26**, 2057–2058 (1990).

[20] E.S. Mok and G.I. Costache, "Skin-Effect Considerations on Transient Response of Transmission Line Excited by an Electromagnetic Pulse," *IEEE Trans. on Electromagnetic Compatibility*, **34**, 320–329 (1992).

[21] K.S. Kunz and R.J. Luebbers, *The Finite Difference Time Domain Method in Electromagnetics*, CRC Press, Boca Raton, FL, 1993.

[22] H.B. Dwight, *Tables of Integrals and Other Mathematical Data*, 4th ed., Macmillan, NY, 1961.

[23] K.R. Shah and Y. Yavin, "Equivalent Representation of Lossy Transmission Lines—Part I" and "Equivalent Representation of Lossy Transmission Lines—Part II: Skin Effect Consideration," *Proc. IEEE*, 1258–1261 (1971).

[24] M.S. Lin, A.H. Engvik, and J.S. Loos, "Measurements of Transient Response on Lossy Microstrips with Small Dimensions," *IEEE Trans. on Circuits and Systems*, **37**, 1383–1393 (1990).

[25] M. Cases and D.M. Quinn, "Transient Response of Uniformly Distributed *RLC* Transmission Lines," *IEEE Trans. on Circuits and Systems*, **27**, 200–207 (1980).

[26] T. Komuro, "Time-Domain Analysis of Lossy Terminations with Arbitrary Terminal Networks," *IEEE Trans. on Circuits and Systems*, **38**, 1160–1164 (1991).

[27] E.C. Chang and S. Kang, "Computationally Efficient Simulation of a Lossy Transmission Line with Skin Effect by Using Numerical Inversion of Laplace Transform," *IEEE Trans. on Circuits and Systems*, **39**, 861–868 (1992).

[28] F.Y. Chang, "Transient Simulation of Nonuniform Coupled Lossy Transmission Lines Characterized with Frequency-Dependent Parameters Part II: Discrete-Time Analysis," *IEEE Trans. on Circuits and Systems*, **39**, 907–927 (1992).

[29] M.S. Ghausi and J.J. Kelly, *Introduction to Distributed-Parameter Networks*, Holt, Rinehart and Winston, NY, 1968.

[30] L. Monroe and C.R. Paul, "Lumped Circuit Modeling of Transmission Lines," *Proc.* 1985 *IEEE International Symposium on Electromagnetic Compatibility*, Wakefield, MA, August 1985, pp. 282–286. (See also L. Monroe, "Modeling of Transmission Lines: A New Iterative, Lumped-Circuit Model," MSEE Thesis, University of Kentucky, May 1985.)

[31] V.K. Tripathi and A. Hill, "Equivalent Circuit Modeling of Losses and Dispersion in Single and Coupled Lines for Microwave and Millimeter-Wave Integrated Circuits," *IEEE Trans. on Circuits and Systems*, **36**, 256–262 (1988).

[32] F.Y. Chang, "Waveform Relaxation Analysis of **RLCG** Transmission Lines," *IEEE Trans. on Circuits and Systems*, **37**, 1394–1415 (1990).

[33] F.Y. Chang, "Waveform Relaxation Analysis of Nonuniform Lossy Transmission Lines Characterized with Frequency-Dependent Parameters," *IEEE Trans. on Circuits and Systems*, **38**, 1484–1500 (1991).

[34] J.I. Alonso, J.B. Borja, and F. Perez, "A Universal Model for Lossy and Dispersive Transmission Lines for Time Domain CAD of Circuits," *IEEE Trans. on Microwave Theory and Techniques*, **40**, 938–946 (1992).

[35] P.S. Yeung, "Lossy Transmission Lines: Time Domain Formulation and Simulation Model," *IEEE Trans. on Microwave Theory and Techniques*, **41**, 1275–1279 (1993).

[36] N. Orhanovic, P. Wang, and V.K. Tripathi, "Generalized Method of Characteristics for Time Domain Simulation of Multiconductor Lossy Transmission Lines," *Proc. IEEE Symposium on Circuits and Systems*, May 1990.

[37] V.K. Tripathi and N. Orhanovic, "Time-Domain Characterization and Analysis of Dispersive Dissipative Interconnects," *IEEE Trans. on Circuits and Systems*, **39**, 938–945 (1992).

[38] J. Mao and Z. Li, "Analysis of the Time Response of Multiconductor Transmission Lines with Frequency-Dependent Losses by the Method of Convolution Characteristics," *IEEE Trans. on Microwave Theory and Techniques*, **40**, 637–644 (1992).

[39] F.-Y. Chang, "The Generalized Method of Characteristics for Waveform Relaxation Analysis of Lossy Coupled Transmission Lines," *IEEE Trans. on Microwave Theory and Techniques*, **37**, 2028–2038 (1989).

[40] A.J. Gruodis, "Transient Analysis of Uniform Resistive Transmission Lines in a Homogeneous Medium," *IBM J. Research and Developmemt*, **23**, 675–681 (1979).

[41] A.J. Gruodis and C.S. Chang, "Coupled Lossy Transmission Line Characterization and Simulation," *IBM J. Research and Development*, **25**, 25–41 (1981).

[42] D.S. Gao, A.T. Yang, and S.M. Kang, "Modeling and Simulation of Interconnection Delays and Crosstalks in High-Speed Integrated Circuits," *IEEE Trans. on Circuits and Systems*, **37**, 1–8 (1990).

[43] T.K. Tang, M.S. Nakhla, and R. Griffith, "Analysis of Lossy Multiconductor Transmission Lines Using the Asymptotic Waveform Evaluation Technique," *IEEE Trans. on Microwave Theory and Techniques*, **39**, 2107–2116 (1991).

[44] J.E. Bracken, V. Raghavan, and R.A. Rohrer, "Interconnect Simulation with Asymptotic Waveform Evaluation (AWE)," *IEEE Trans. on Circuits and Systems*, **39**, 869–878 (1992).

## PROBLEMS

**5.1** Show, by direct substitution, that (5.3) satisfy the transmission-line equations given in (5.2).

**5.2** Consider a lossless two-conductor line that has $R_S = 300\,\Omega$, $R_L = 60\,\Omega$, $Z_C = 100\,\Omega$, $v = 200$ m/μs, $\mathscr{L} = 200$ m, and $V_S(t) = 400u(t)$ where $u(t)$ is the unit-step function. Sketch $V(0, t)$, $I(0, t)$, $V(\mathscr{L}, t)$, $I(\mathscr{L}, t)$ for $0 \leq t \leq 10\,\mu$s. Do the results converge to the expected steady-state values? Confirm your results using SPICE.

**5.3** Repeat Problem 5.2 for $R_L = 0$ (short-circuit load).

**5.4** Repeat Problem 5.2 for $R_L = \infty$ (open-circuit load).

**5.5** A time-domain reflectometer (TDR) is an instrument used to determine properties of transmission lines. In particular, it can be used to detect the locations of imperfections such as breaks in the line. The instrument launches a pulse down the line then records the transit time for that pulse to be reflected at some discontinuity and to return to the line input. Suppose a TDR having a source impedance of $50\,\Omega$ is attached to a $50\,\Omega$ coaxial cable having some unknown length and load resistance. The dielectric of the cable is Teflon ($\varepsilon_r = 2.1$). The open-circuit voltage of the TDR is a pulse of duration $10\,\mu$s. If the recorded voltage at the input of the TDR is as shown in Fig. P5.5, determine the length of the cable and the unknown load resistance. Confirm your results using SPICE.

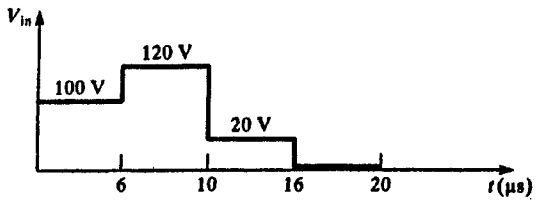


FIGURE P5.5

5.6 A 12 V battery ($R_S = 0$) is attached to an unknown length of transmission line that is terminated in a resistance. If the current to that line for 6 μs is as shown in Fig. P5.6, determine the line characteristic resistance and the unknown load resistance. Confirm your results using SPICE.

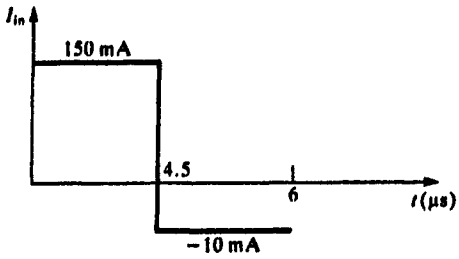


FIGURE P5.6

5.7 Digital data pulses should ideally consist of rectangular pulses. Actual data, however, have a trapezoidal shape with certain rise/fall times. Matching the data transmission line eliminates reflections and potential logic errors arising from these reflections. However, matching cannot always be accomplished. In order to investigate this problem, consider a line having $R_S = 0$ and $R_L = \infty$. Assume that the source voltage $V_S(t)$ is a ramp waveform given by

$$V_S(t) = \begin{cases} 0 & \text{for} \quad t \leq 0 \\ \dfrac{t}{\tau_r} & \text{for} \quad t \leq \tau_r \\ 1 & \text{for} \quad t \geq \tau_r \end{cases}$$

where $\tau_r$ is the risetime of the pulse. Sketch the load voltage for line

lengths having one-way transit times $T$ such that:

1. $\tau_r = \frac{1}{10}T$
2. $\tau_r = 2T$
3. $\tau_r = 3T$
4. $\tau_r = 4T$.

This example shows that in order to avoid problems resulting from mismatch, one should choose line lengths short enough for $\tau_r$ to be $\gg T$ for the desired data. Confirm your results using SPICE.

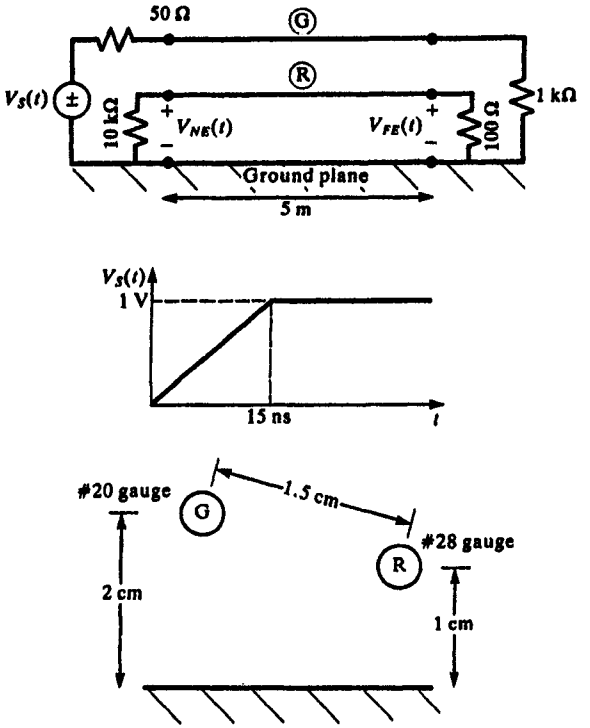


FIGURE P5.8

5.8 Consider the three-conductor line shown in Fig. P5.8. The driven or generator conductor is a #20 gauge solid wire (radius 16 mils) and the pickup or receptor wire is a #28 gauge solid wire (radius 6.3 mils). The wires are separated by 1.5 cm and are suspended above an infinite, perfectly conducting ground plane at heights of 2 cm and 1 cm as shown.

The lines are terminated as shown and driven by a ramp voltage source. Neglect all losses, assume a homogeneous medium and compute and plot versus time the near-end and far-end coupled voltages, $V_{NE}(t)$ and $V_{FE}(t)$, by the following methods:

1. SPICE model
2. Branin's method
3. The time-domain to frequency-domain transformation method
4. The finite difference method.

**5.9** Verify, by long division, the results given in (5.29).

**5.10** Use the Bergeron diagram method to verify the results of Problem 5.2.

**5.11** Diagonalize the following inductance matrix for a homogeneous medium via the method of Section 5.2.1.1:

$$\mathbf{L} = \begin{bmatrix} 5 & 1 \\ 1 & 3 \end{bmatrix} \mu\text{H/m}$$

**5.12** Diagonalize the product **CL** using the method of Section 5.2.1.2 using **L** given in Problem 5.11 and

$$\mathbf{C} = \begin{bmatrix} 10 & -5 \\ -5 & 15 \end{bmatrix} \text{pF/m}$$

**5.13** A three-conductor line in an inhomogeneous medium is characterized with **C** and **L** of Problem 5.12. The total length is 2 m and is terminated in 1 kΩ resistors and driven by a 50 Ω 1 V pulse source having a 10 ns rise time. Solve for the terminal crosstalk voltages using:

1. SPICE
2. Branin's method
3. The time-domain to frequency-domain transformation method
4. A lumped-pi circuit
5. The FDTD method.

**5.14** Verify the relations in (5.94).

**5.15** Derive the Fourier series coefficients for a trapezoidal waveform given in (5.100).

**5.16** Derive the FDTD results given in (5.120).

**5.17** Verify the relations given in (5.151).

**5.18** Derive the recursion relation given in (5.156).

**5.19** Plot the time-domain step response for the lossy PCB shown in Fig. 5.42 for a zero source impedance and a matched line using the low-loss result in (5.169).

**5.20** Determine the impulse response for Problem 5.19 using (5.179).

**5.21** Examine how you would implement the time-domain result shown in Fig. 5.46 using the results of Table 5.2 and (5.189).

**5.22** Determine the time-domain crosstalk for a three-conductor PCB having $w = s = 8$ mils and a board having a thickness of 10 mils and $\varepsilon_r = 12$. The line length is 15 cm and the terminations are 1 kΩ resistors. The source is a 1 V trapezoidal pulse train shown in Fig. 5.29 having a 50 Ω source resistance and 50 ps rise/fall times. Compare the lossy and lossless cases using:

1. The SPICE model
2. The time-domain to frequency-domain transformation
3. A lumped-pi structure
4. The FDTD model.